ELECTRICAL POWER GENERATION
FROM STANDING SHOCK WAVES

by

JOHN BEVERLY PEARSON

B.Sc., Queen's University, 1976

A THESIS SUBMITTED IN PARTIAL FULFILMENT OF

THE REQUIREMENTS FOR THE DEGREE OF

MASTER OF APPLIED SCIENCE

in

THE FACULTY OF GRADUATE STUDIES

(Department of Physics)

We accept this thesis as conforming

to the required standard

THE UNIVERSITY OF BRITISH COLUMBIA

December 1979

In presenting this thesis in partial fulfilment of the requirements for an advanced degree at the University of British Columbia, I agree that the Library shall make it freely available for reference and study. I further agree that permission for extensive copying of this thesis for scholarly purposes may be granted by the Head of my Department or by his representatives. It is understood that copying or publication of this thesis for financial gain shall not be allowed without my written permission.

Department of Physics

The University of British Columbia
2075 Wesbrook Place
Vancouver, Canada
V6T 1W5

Date December 31, 1979

ABSTRACT

Standing shock waves in a supersonic flow field produce density gradients across which an electrical potential is established. If electrodes are mounted upstream and downstream of the standing shock, an electrical current can be extracted. The electrical power output by such a system (called a bow shock generator) has been measured. To produce the supersonic flow an overdriven detonation shock tube, capable of producing Mach 12 shocks in 5 Torr argon, was constructed and used as a short duration supersonic wind tunnel. The open circuit voltage of a single bow shock generator with a 2 cm electrode separation was measured to be 0.95 V, and the maximum power output to 53 mW. By reducing the electrode separation to 1 cm the maximum power output was increased to 90 mW, while the open circuit voltage remained unchanged. It was found that when two bow shock generators are mounted side by side in the flow a parallel connection of their outputs produced a small increase in current. However no increase in output voltage was observed when the generators were connected in series. It was also found that when an oblique shock and its reflection from the wall were connected together in series, the output voltage was less than that of the oblique shock alone. However this was likely due to a short circuit path between the electrodes through the boundary layer. Some of the measurements were inconclusive due to an insufficiently long test time. A preliminary analysis was

done on a system in which a set of bow shock generators is used as a topping system for a conventional electrical generation system. It was shown that the bow shock generators must be operated at very low Mach numbers if they are to be efficient in this application.

TABLE OF CONTENTS

LIST OF TABLES

LIST OF FIGURES

FIGURE PAGE

FIGURE PAGE

ACKNOWLEDGEMENTS

I would like to express my thanks to my supervisor, Dr. B. Ahlborn, for suggesting this project and for his help and encouragement throughout the work. I would also like to thank Dr. F. Curzon for his helpful discussions and his suggestions during the completion of this work. Also all the members of the Plasma Physics Group, faculty members and students alike, were always willing to discuss problems and offer encouragement.

A. Cheuck has been very good at designing and building electronic equipment for the shock tube and for diagnostics. His willingness to provide prompt attention in the repair or adjustment of any equipment was most appreciated.

I also wish to thank the members of the main machine shop, particularly Mr. P. Hass and Mr. O. Christiansen, for the machining of the shock tube and the driver section and Mr. C. Sedger of the student shop for his assistance and suggestions throughout the project.

Finally I wish to thank my wife, Janet, for her assistance in the preparation of this report.

CHAPTER 1. INTRODUCTION

1.1 PRINCIPLE OF THE BOW SHOCK GENERATOR

The existence of space charge layers and electric fields inside ionizing shock fronts has been known for some time and a number of experiments have measured the voltage across a free running shock[1,2].

In a free running shock the moving space charge layer also has a magnetic field associated with it[3]. An understanding of these features of shock fronts is important to a variety of fields including laser fusion experiments, stellar formation, and direct energy conversion[4].

The voltage across the shock arises because of the strong pressure and ionization gradients in the shock front. Driven by these gradients the electrons behind the shock diffuse forward away from the region of high concentration. Because the ions have a much lower mobility, they remain more or less fixed and a charge separation develops. An equilibrium is reached when the electric field induced by the charge separation balances the gradient term driving the diffusion. This electric field embedded in the shock front results in a potential difference across the shock. A representation of the variation of these quantities across a shock front is shown in Figure 1.1[4].

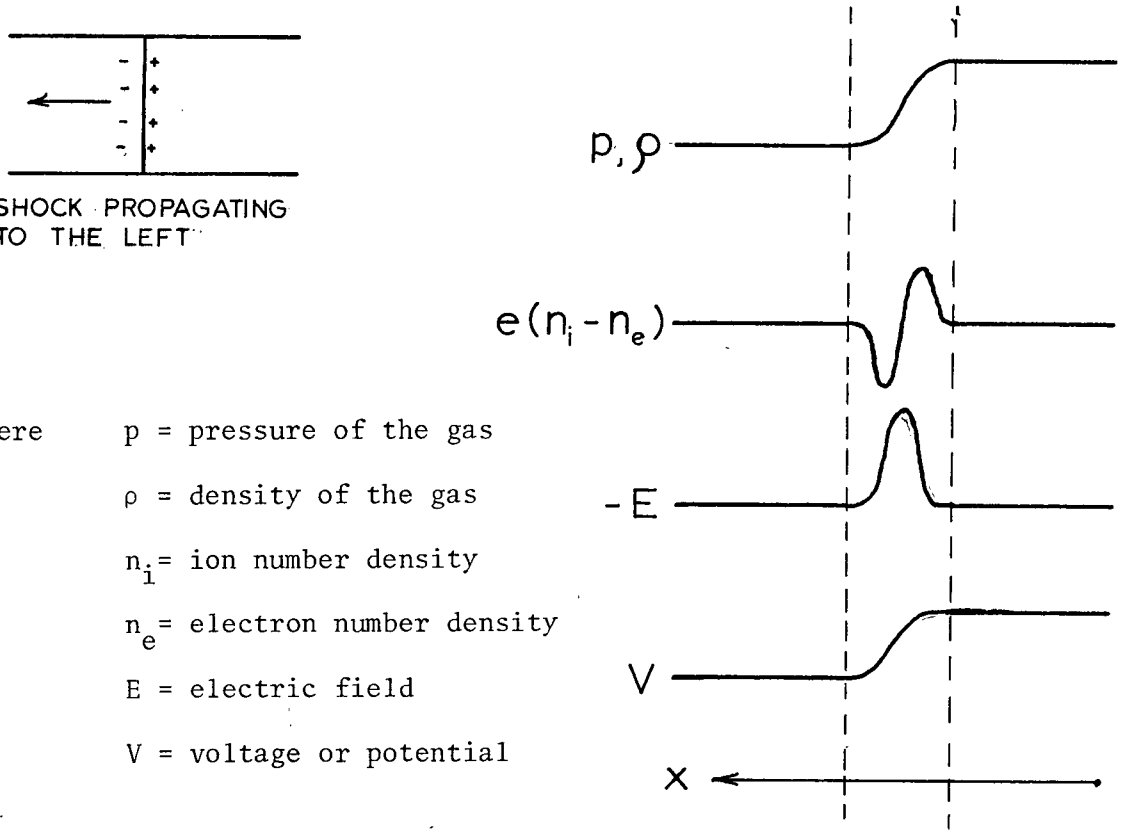

where p = pressure of the gas

ρ = density of the gas

n_i = ion number density

n_e = electron number density

E = electric field

V = voltage or potential

Figure 1.1 A representation of the structure of an ionizing shock front

In order to make measurements of the electromagnetic effects more easily a shock front which is stationary in the lab frame would be desirable. Such a shock may be generated by directing a supersonic gas flow onto a fixed obstacle to create a standing bow shock. The voltage across the shock can easily be measured by placing one electrode on each side of the standing shock. Furthermore, if these electrodes are connected to a load the potential across the shock can be made to drive a current through the load. In this way a standing shock can be used to extract electrical energy directly from a flow of hot gas. Such a device is termed a "bow shock generator"[5]. The voltage output of a bow shock generator has

been measured[4,6] and was found to be typically about 1 volt. These particular measurements also indicated a short circuit current of approximately 100mA.

A bow shock generator can in principle operate in a temperature regime well above the range of conventional thermodynamic engines such as turbines. This is a temperature regime where to date only Magnetohydrodynamic machines have been proposed for direct energy conversion. In order to make the bow shock generator a practical device for the direct conversion of electrical power one would like to increase the output voltage or current. The aim of this thesis was to see if this could be done by connecting together the outputs from more than one shock generator. Connections between shocks were investigated in two basic geometries (see Figure 1.2):

(1) connections between several shocks which stood side by side in the flow (both series and parallel electrical connections)

(2) a connection of several shocks formed by one shock and its successive reflection from the walls (series electrical connection).

Another important aim of this work was to define a useful figure of merit for the bow shock generators so that their performance in these tests could be compared to that of other systems.

To create a standing bow shock suitable for use in the tests outlined above one must have an incident flow which

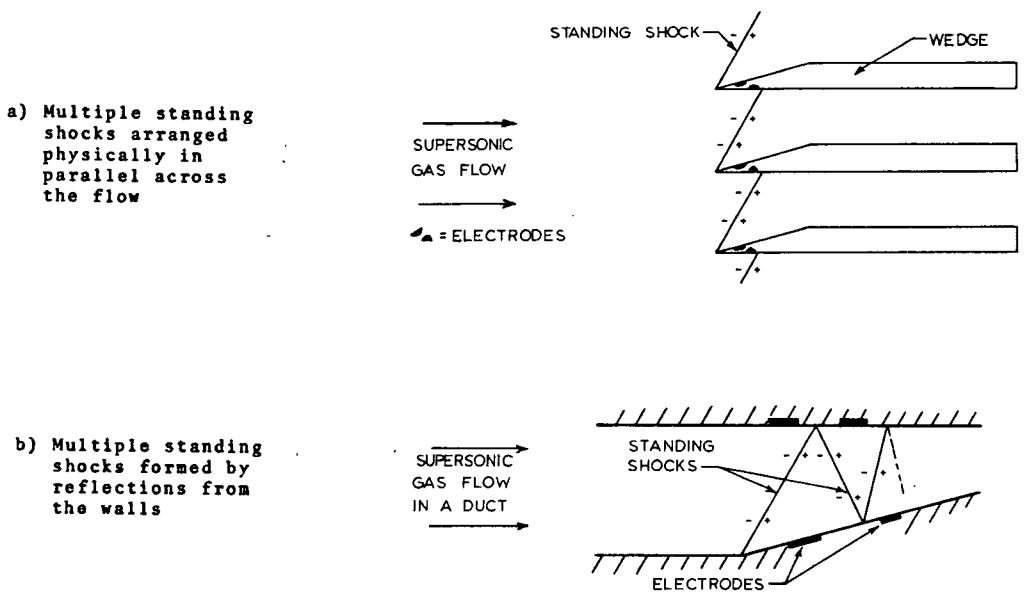

Figure 1.2 The two geometries used to investigate multiple shock connections

meets a number of requirements. These may be summarized as follows:

1) The flow must consist of gas in a well defined thermodynamic state.
2) The flow must be supersonic.
3) The duration of the flow must be at least 10 microseconds to allow time for measurements to be made.
4) The flow should show an increase of ionization on passing through the standing shock.
5) There should be no electrical currents present in the initial flow.

This thesis is divided into two main parts. The first part (Chapters 1 to 4) deals with the theory, construction, and testing of a device which generates a suitable supersonic flow field while the second part (Chapters 4 to 8) deals with

the investigations and analysis of the bow shock generators.

In Chapter 2 a method of generating a suitable flow using an imploding detonation shock tube is developed. Chapter 3 describes the construction and preliminary testing of the shock tube. The design and construction of the generator systems is outlined in Chapter 4. Chapter 5 describes the experiments in which several generators were connected together. The results from these experiments are included in this chapter along with those from some tests on individual shock generators. All of these results are summarized in Chapter 6 and an attempt is made to interpret some of them theoretically. In Chapter 7 a useful figure of merit (the effectiveness) is defined for the generators and a typical value is quoted. In addition a comparison is made between the performance of a hybrid bow shock generator/conventional turbine generation system and that of a strictly conventional system. Chapter 8 contains a summary of the original contributions made by the author, as well as the conclusions and suggestions for further work.

CHAPTER 2. PRODUCTION OF A SUITABLE TEST FLOW WITH AN OVERDRIVEN DETONATION SHOCK TUBE

The experiment outlined in Chapter 1 requires a supersonic flow of gas that is in a well defined thermodynamic state. When an obstacle is inserted into the flow so that a standing shock is created the ionization in the flow must increase significantly across the shock. The flow must also be free of large electrical currents.

One of the simplest ways of generating a suitable test flow would be to use the flow behind a shock wave in argon. The thermodynamic state of a gas behind a shock is well defined and argon is one of the simplest and best understood gases. If the shock wave is made strong enough the flow behind it can become supersonic in the lab frame. In this way a shock tube can be used as a short duration supersonic wind tunnel. The supersonic flow of argon at any point in such a wind tunnel lasts from the time the shock wave arrives until the time the contact surface arrives. The Mach number for the flow behind the shock front depends on the strength of the shock, and can be obtained from the Rankine-Hugoniot conservation equations which apply to gas flowing through the shock front.

2.1 SUPERSONIC FLOW BEHIND A SHOCK WAVE

The conservation equations for the flow across a shock front may be written in the frame of reference of the shock as[7]:

$$\text{mass:} \quad \rho_1 u_1' = \rho_2 u_2' \tag{2.1}$$

$$\text{momentum:} \quad p_1 + \rho_1 u_1'^2 = p_2 + \rho_2 u_2'^2 \tag{2.2}$$

$$\text{energy:} \quad h_1 + \tfrac{1}{2}u_1'^2 = h_2 + \tfrac{1}{2}u_2'^2 \tag{2.3}$$

where the primes indicate that the quantities are measured in the shock front frame and the variables are defined as shown in Figure 2.1. An equivalent representation of the shock in the lab frame is also shown in Figure 2.1. The equation of state for the gas is initially taken to be that for a simple ideal gas[7](constant specific heat, no ionization, monatomic)

$$h = \frac{\gamma}{\gamma+1}\frac{p}{\rho} \tag{2.4}$$

where γ is the adiabatic exponent equal to c_p/c_v. If the

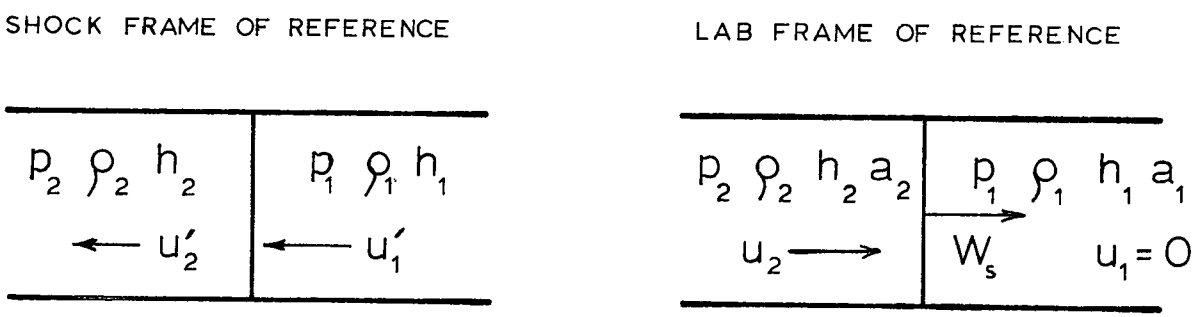

where W_s = shock speed
u^s = local gas velocity
T = local gas temperature
p = gas pressure
ρ = gas density
a = local sound speed

and $u_2 = W_s - u_2'$
$u_1^2 = W_s^s$

Figure 2.1 The flow across a shock front

shock propagates into stationary gas the initial velocity in the shock frame, u_1', is equal to the shock speed W_s. Using the initial conditions in the stationary gas the four equations (2.1) through (2.4) may be solved keeping ($u_1' = W_s$) the shock speed as the free parameter. If this shock speed is normalized to the sound velocity in the gas ahead of the shock by defining the Mach number (M_1)

$$M_1 = \frac{u_1'}{a_1} = \frac{W_s}{a_1} \qquad (2.5)$$

then the well known shock relations are found.

$$\frac{\rho_2}{\rho_1} = \frac{(\gamma+1)M_1^2}{2+(\gamma-1)M_1^2} = \frac{u_1'}{u_2'} \tag{2.6}$$

$$\frac{p_2}{p_1} = \frac{2\gamma M_1^2-(\gamma-1)}{\gamma+1} \tag{2.7}$$

$$\frac{T_2}{T_1} = \frac{(2\gamma M_1^2-(\gamma-1))(2+(\gamma-1)M_1^2)}{(\gamma+1)^2 M_1^2} \tag{2.8}$$

A figure of merit for the flow generated behind a shock wave is provided by the local Mach number $M_2=u_2/a_2$. This is the Mach number of the flow in the lab frame. M_2 is related to the Mach number of the shock front ($M_1=W_s/a_1$, see Figure 2.1) by the following expression, which may be obtained by suitable combinations of the above results[7].

$$M_2 = \frac{u_2}{a_2} = \frac{2(M_1^2-1)}{(2\gamma M_1^2-\gamma-1)^{\frac{1}{2}}(2+(\gamma-1)M_1^2)^{\frac{1}{2}}} \tag{2.9}$$

This function is plotted in Figure 2.2. It should be noted that M_2 has an upper bound which is practically reached with shock speeds (M_1) of about Mach 10. From equation 2.9 the upper limit for M_2 may be seen to be

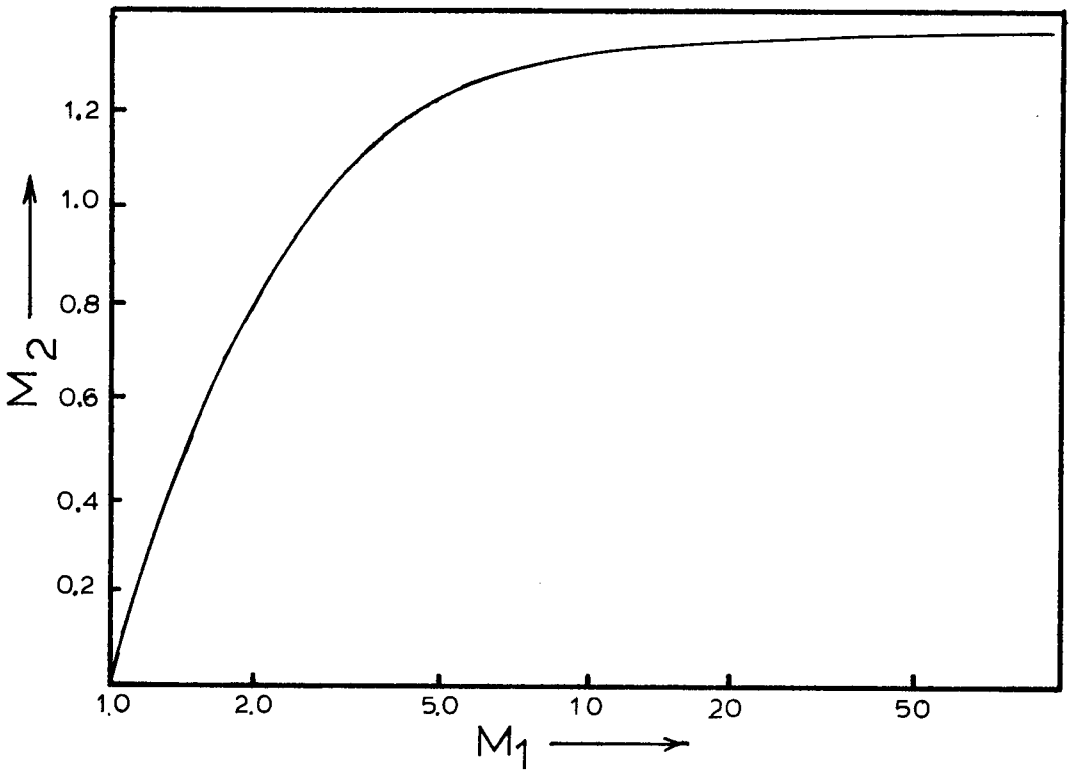

Figure 2.2 The local Mach number of the shock heated gas (M_2) as a function of the shock Mach number (M_1).

$$M_{2max} = \lim_{M_1 \to \infty}(M_2) = \left[\frac{2}{\gamma(\gamma-1)}\right]^{\frac{1}{2}} \qquad (2.10)$$

For an ideal monatomic gas with γ=1.67 the highest Mach number which may be achieved in the flow behind a shock is M_2=1.35. If the gas is ionized by its passage through the shock wave γ is no longer a constant and, in fact, it becomes somewhat

smaller. In this case the highest available Mach number would be slightly higher (1.63).

2.2 THE REQUIREMENT OF IONIZATION INCREASE ACROSS THE STANDING SHOCK

While it is possible to generate a supersonic flow with a shock wave, for the purpose of these experiments the flow must also satisfy another requirement, that of showing an increase in ionization on passing through a standing shock. Since it is not possible to produce high Mach number flows, a standing shock (created by inserting an obstacle into the flow) will be relatively weak. This means that the jump in the temperature of the flow across the standing shock will be fairly small.

The variation of the degree of ionization, α, with temperature and pressure is shown for a gas with an ionization energy of 15 eV in Figure 2.3[8]. From this data it can be seen that the most rapid change of ionization with temperature is obtained if α is in the range 5-95%. In this partially ionized regime the degree of ionization is very sensitive to temperature and thus even a weak standing shock will increase the ionization substantially. If a shock tube is to be used to produce the supersonic flow for the study of bow shock generators it is therefore important that the incident shock be of sufficiently high Mach number to produce partial ionization in the argon behind it.

When ionization becomes significant the calculation of

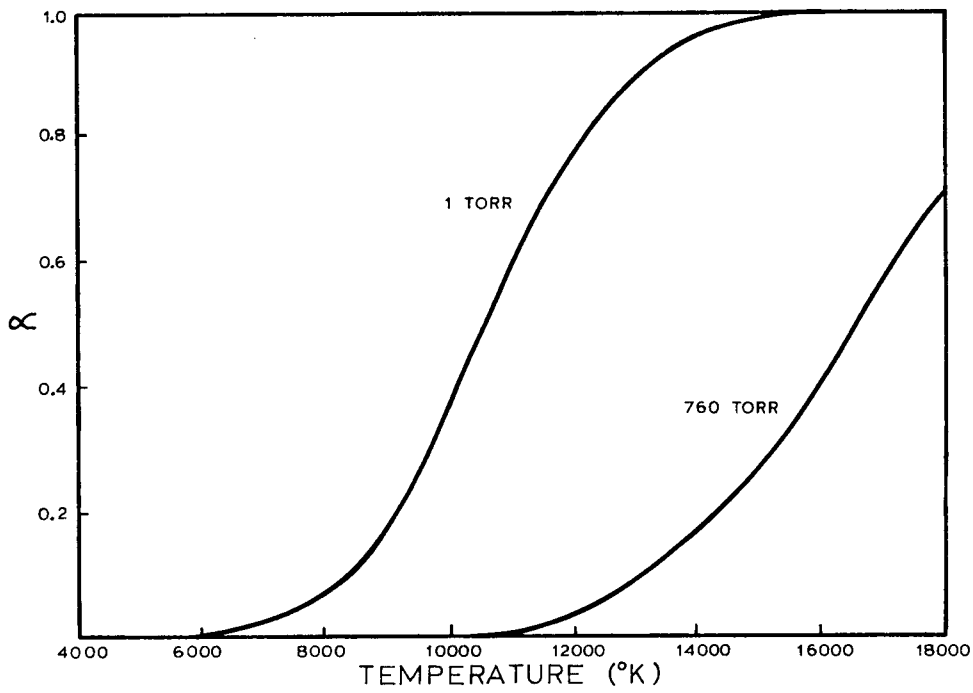

Figure 2.3 Fractional ionization (α) of a gas with an ionization energy of 15 eV as a function of temperature.

the thermodynamic parameters behind the shock front becomes somewhat more complicated[9]. In a partially ionized gas γ is no longer a constant independent of the pressure and temperature and the equation of state (2.4) is no longer applicable. Furthermore the coefficient γ cannot serve to represent both the specific heat ratio, c_p/c_v, and the enthalpy coefficient. Therefore for use in the equation of state the new enthalpy coefficient, g, is defined[9]. With this coefficient, which is a function of the thermodynamic variables, the equation of state may be written as

$$h = \frac{g}{g-1}\frac{p}{\rho} = \frac{g(h,p)}{g(n,\rho)-1}\frac{p}{\rho} \qquad (2.11)$$

If the function g(h,p) is known from thermodynamic data, the three conservation equations, (2.1) through (2.3), and the new equation of state, (2.11), may be solved by an iterative method leaving the Mach number as a parameter. Details of this method are described in Appendix A. In this way the thermodynamic variables behind partially ionizing shock fronts may be calculated. Of these variables the temperature and the degree of ionization are of the most immediate interest. Figure 2.4[10] shows the temperature and degree of ionization behind a shock wave propagating into argon as a function of Mach number. The values are shown for a number of initial argon pressures. An examination of the graph shows that if

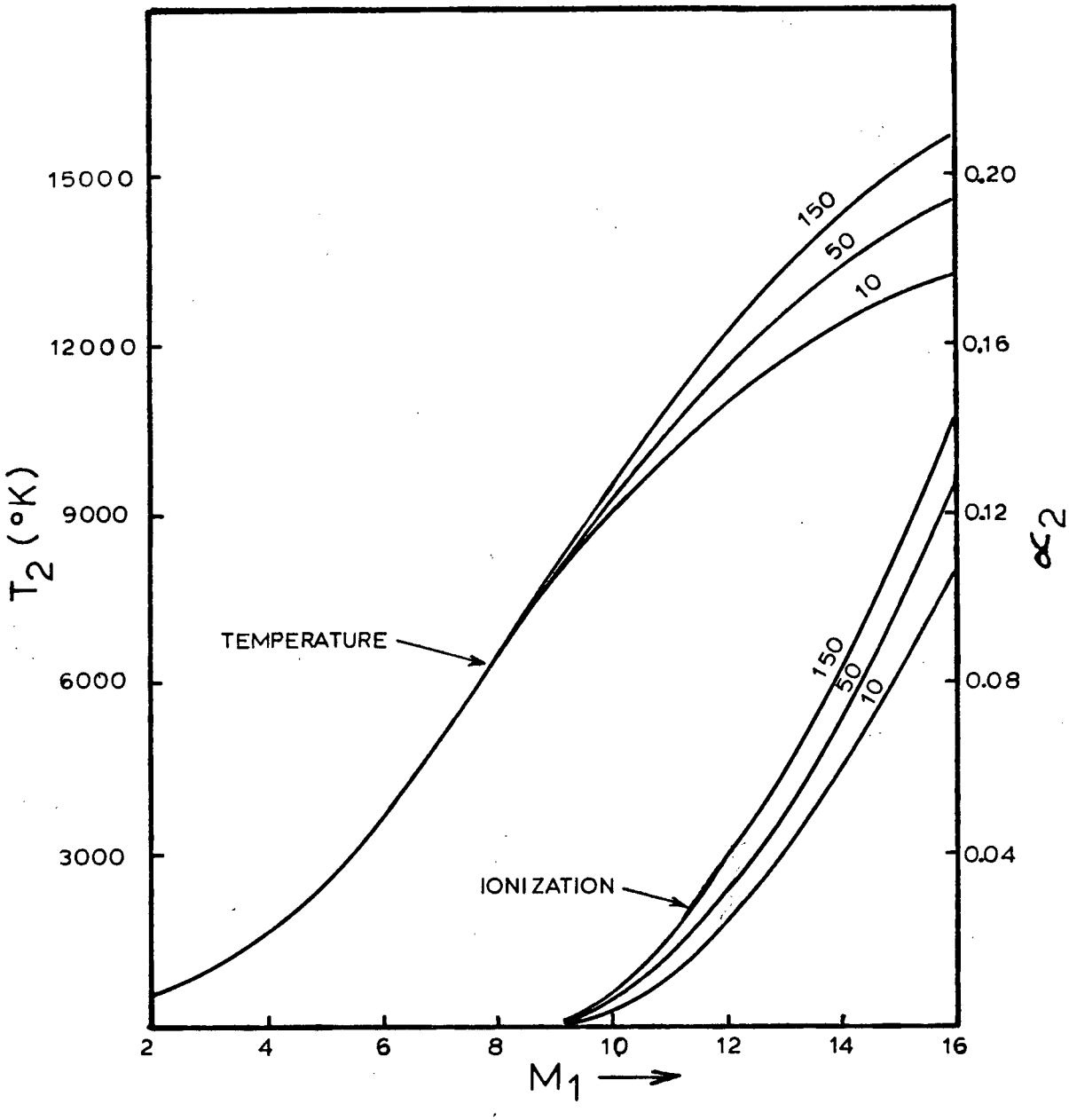

Figure 2.4 Temperature (T_2) and degree of ionization (α_2) in the flow behind a shock wave in argon. The figures on the graphs are the initial pressure ahead of the shocks.

there is to be significant ionization in the flow behind the shock then the shock speed must be at least Mach 11. If an obstacle is inserted into the flow behind a Mach 11 shock wave a standing shock will be created and the ionization in the flow will be significantly increased across the shock.

2.3 THE DIAPHRAGM SHOCK TUBE

In order to satisfy the requirements for the test flow, a shock tube capable of producing a Mach 11 shock is needed. To see what features are necessary for a shock tube to produce such high Mach numbers the operation of a conventional diaphragm shock tube is first discussed. For the purposes of this section $\gamma=g$ is assumed to be constant.

Figure 2.5 shows a diagram of a diaphragm shock tube. The driver section on the left is filled with a high pressure gas while the low pressure section on the right is filled with the test gas. A diaphragm separates the two sections. When this diaphragm is caused to burst, a shock wave travels down the shock tube into the test gas while a rarefaction wave moves back into the driver. These features are shown in the X-T diagram above the shock tube. At some time, T, after the diaphragm has opened one would find a velocity and pressure distribution in the shock tube similar to that shown at the bottom of Figure 2.5.

The speed of the shock may be related to the initial conditions in the high and low pressure sections in the

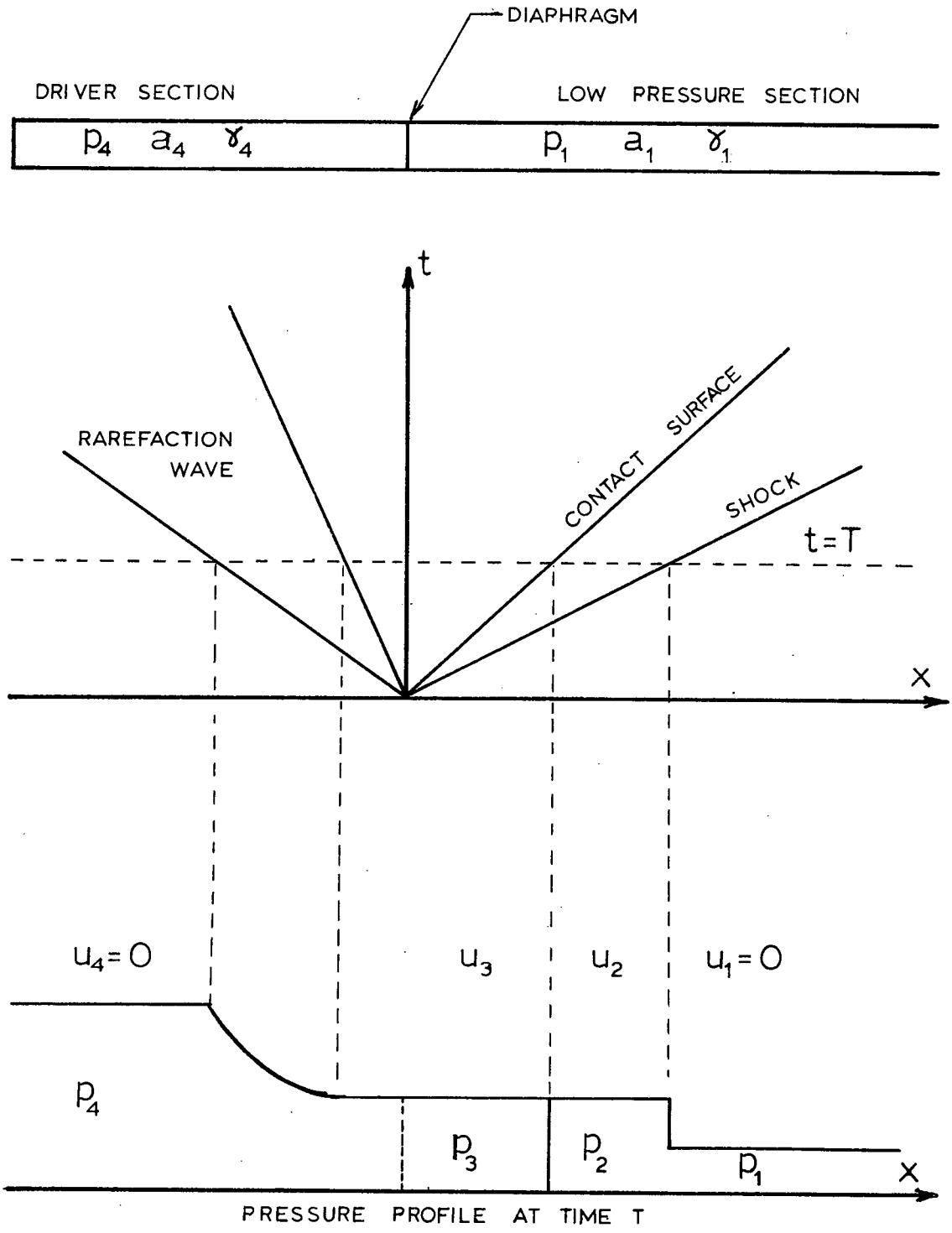

Figure 2.5 The diaphragm shock tube

following way. The initial conditions in the low pressure section, region 1, may be related to those in region 2 by the shock relations with the Mach number, M_1, as a parameter. If it is assumed that the pressure and velocity are constant across the contact surface, the conditions in region 2 can be related to those in region 3. Finally, to relate region 3 to the initial conditions in the high pressure section, region 4, the rarefaction wave is assumed to be isentropic. In this way the initial conditions in the low pressure section have been related to those in the high pressure section with the Mach number (M_1) as a parameter. The initial pressure ratio across the diaphragm p_4/p_1 that is needed to obtain a shock of Mach number M_1 can therefore be expressed as

$$\frac{p_4}{p_1} = \frac{2\gamma_1 M_1^2 - (\gamma_1 - 1)}{\gamma_1 + 1} \left[1 - \frac{\gamma_4 - 1}{\gamma_4 + 1} \frac{a_1}{a_4} \left(M_1 - \frac{1}{M_1} \right) \right]^{-\frac{2\gamma_4}{\gamma_4 - 1}} \qquad (2.12)$$

The diaphragm pressure ratio is plotted as a function of Mach number for several sound speed ratios a_4/a_1 in Figure 2.6. An examination of the equation (2.12) or the graph shows that in order to achieve high Mach number shocks, a high diaphragm pressure ratio, p_4/p_1, and a high sound speed ratio, a_4/a_1, are needed.

The initial fill pressure of argon on the low pressure side of the diaphragm was 5 Torr. This value was chosen to obtain high diaphragm pressure ratios but still maintain a

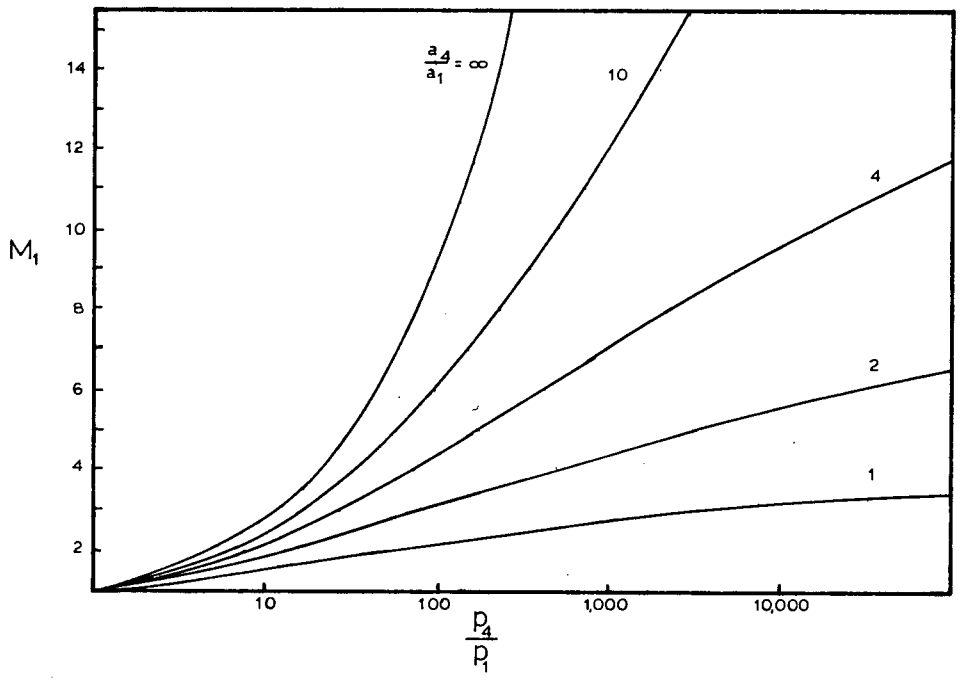

Figure 2.6 The relationship between diaphragm pressure ratio (p_4/p_1) and Mach number (M_1) shown for a variety of sound speed ratios (a_4/a_1)

substantial density in the gas behind the shock. The pressure required in the driver section to generate a Mach 11 shock can be calculated from these initial conditions and equation (2.12). For approximate calculations the graph in Figure (2.6) may be used. If helium is used as a driver gas the pressure in the driver would have to be 2000 atmospheres. This was judged to be too large a pressure to be handled in any reasonably sized experiment. By using a gas with a higher sound speed, such as hydrogen, the driver pressure could be reduced to 65 atmospheres. However the use of high pressure hydrogen was considered to be too dangerous because we do not have the facilities to handle high pressure hydrogen safely.

High Mach number shocks may also be generated by increasing the sound speed in the driver gas through heating. The electrothermal shock tube is one device which uses this principle. Unfortunately it is known[12] that electrical signals may be picked up almost anywhere in an electrothermal shock tube. These signals would make the detection and interpretation of bow shock generator signals exceedingly difficult. Therefore this type of shock tube was immediately ruled out. Another means of heating the driver gas is to fill the driving section with a combustible mixture of gases and to ignite the mixtures. After the reaction is complete the driver will be filled with high pressure, high temperature gas.

2.4 OVERDRIVEN DETONATION SHOCK TUBE

It has been demonstrated in this lab[13] that a simple and effective shock tube, capable of producing high Mach number shock waves, can be built with an overdriven detonation driver. In this device the combustible mixture of driver gases is heated and raised to a high pressure by a detonation wave. The driver section for such a shock tube has a special geometry as shown in Figure(2.7). A detonation wave is initiated at one end of the chamber with a strong spark and propagates up to the midplane of the driver as a Chapman-Jouget detonation. Beyond this point the wave is forced into a converging channel and it becomes an overdriven[13], or strong[14], detonation. The diaphragm bursts shortly after the detonation has been reflected from it and a shock wave is driven into the low pressure gas.

The main advantage of the overdriven detonation driver is that the pressure and temperature behind an overdriven detonation are higher[15] than those those available with other combustion processes. This makes such a driver very attractive for producing high Mach number shocks.

While it is relatively easy to produce a shock of speed Mach 11 in an overdriven detonation shock tube the flow of argon behind the shock may not be completely uniform. There are several potential causes of unsteadiness in this flow. A detonation wave is, in general, followed by a centred rarefaction wave where the pressure is decreased. While the

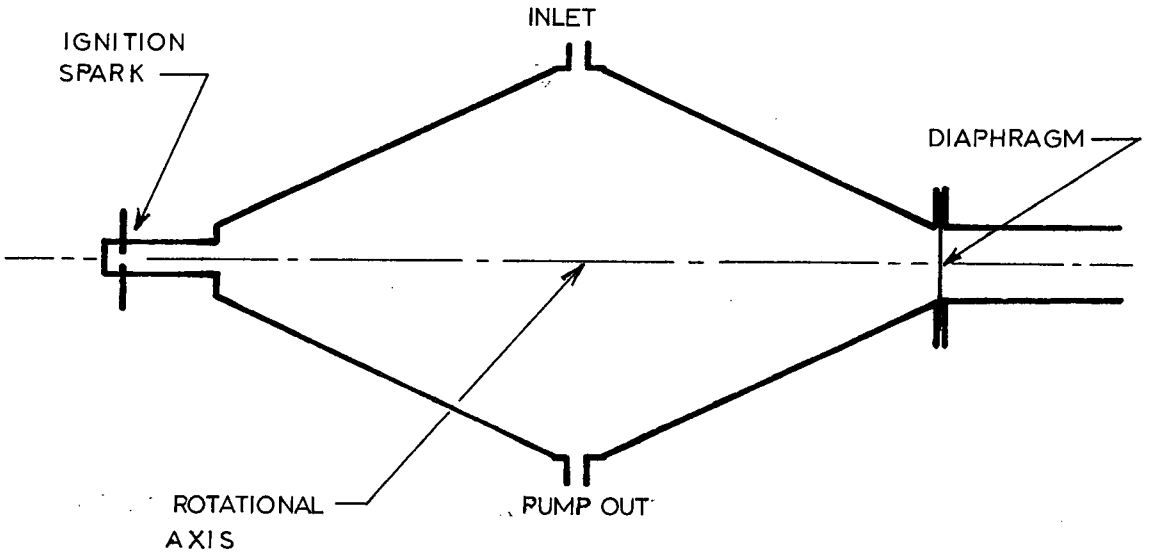

Figure 2.7 An axial secton of the shock tube driver (schematic).

area convergence in the driver section helps to "fill in" some of this decrease the pressure in the driver will not be completely uniform when the diaphragm bursts. In addition, studies of imploding detonation have shown that the gas behind the reflected detonation is not at rest. Figure (2.8) shows a smear camera photograph of a sector of a cylinrical imploding detonation[16]. It can be seen that the particle paths behind the reflected detonation move away from the axis. The fact that both the pressure and the gas velocity in the driver section will be nonuniform when the diaphragm ruptures may introduce disturbances into the flow behind the shock. These disturbances will be in the form of compression or rarefaction

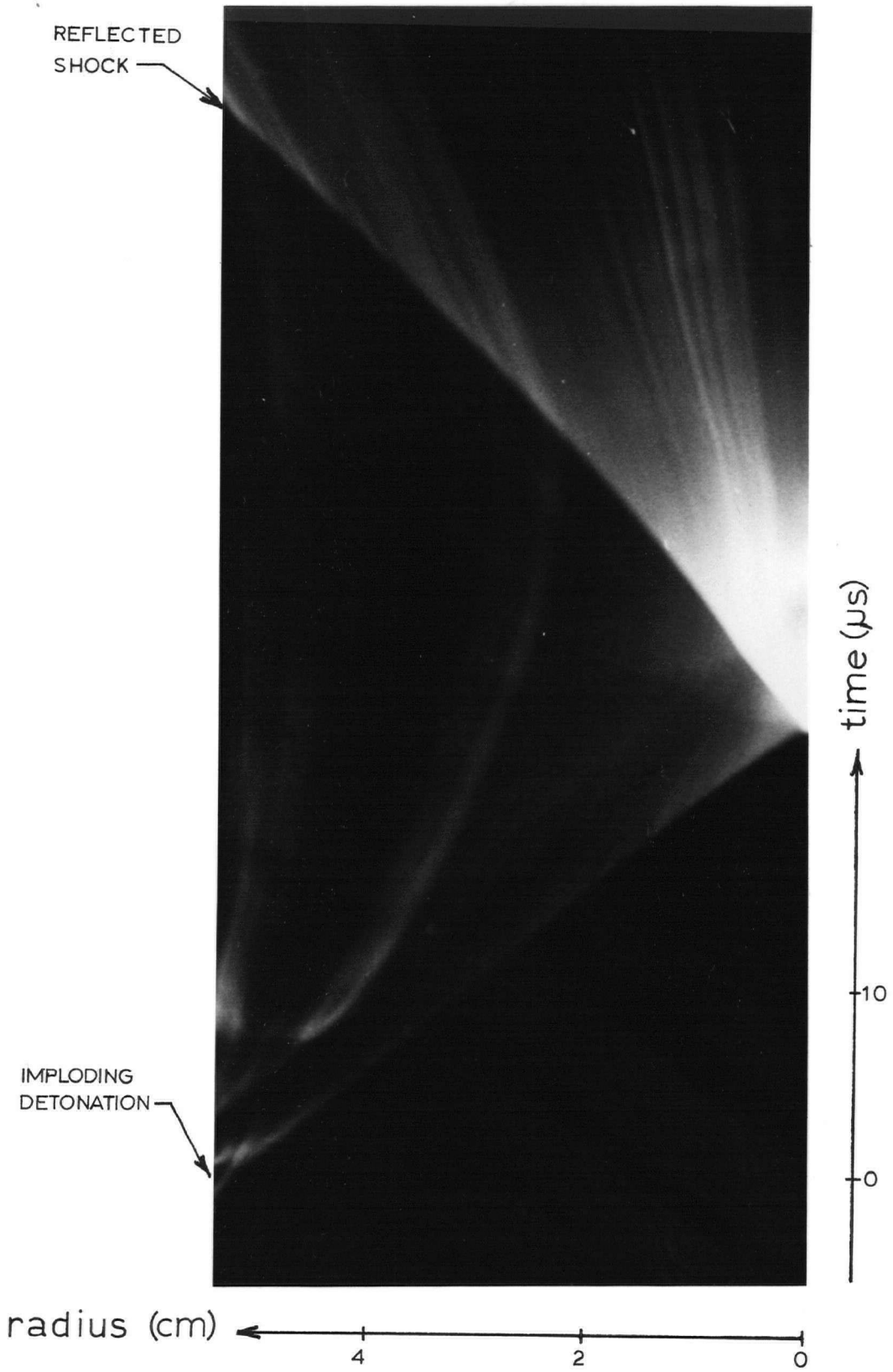

Figure 2.8 A smear camera photograph of one sector of a cylindrical imploding detonation

waves which propagate down the shock tube. They will first influence the pressure and velocity of the slug of test gas and somewhat later they will affect the speed of the shock front itself.

2.5 SUMMARY

It should be possible to meet most of the requirements for the test flow outlined in the introduction (Chapter 1) by using the flow behind a Mach 11 shock wave in argon. This flow will be supersonic and it is possible to create a standing shock in which the degree of ionization of the flow is increased (from approximately 2.7% to 5%). By using a shock tube with an overdriven detonation driver a shock of speed Mach 11 may be obtained. The only shortcoming of this device is that flow behind shocks generated in this manner may show some unsteady features. This type of shock tube was selected however because its operation was free from large electrical currents and its design was simple.

CHAPTER 3. CONSTRUCTION AND DEVELOPMENT OF THE SHOCK TUBE

3.1 CONSTRUCTION OF THE SHOCK TUBE

3.1.1 The Facility

In the previous chapter it was pointed out that a shock tube with a hot driver gas was required in order to study the extraction of electrical power from standing shock waves. Using the experience with detonation shock tubes acquired in this lab[13] it was decided to construct such a device. A schematic diagram of the entire system is shown in Figure 3.1. The main features of this new facility are that it has a square cross section with an area of one square inch and an overall length of approximately two metres. The shock tube was built in sections so that a short test section could be inserted into the tube at a variety of distances from the diaphragm. The driver section is of the imploding detonation type, using oxy-acetylene as the driver gas. An acetate diaphragm separates the driver section from the shock tube.

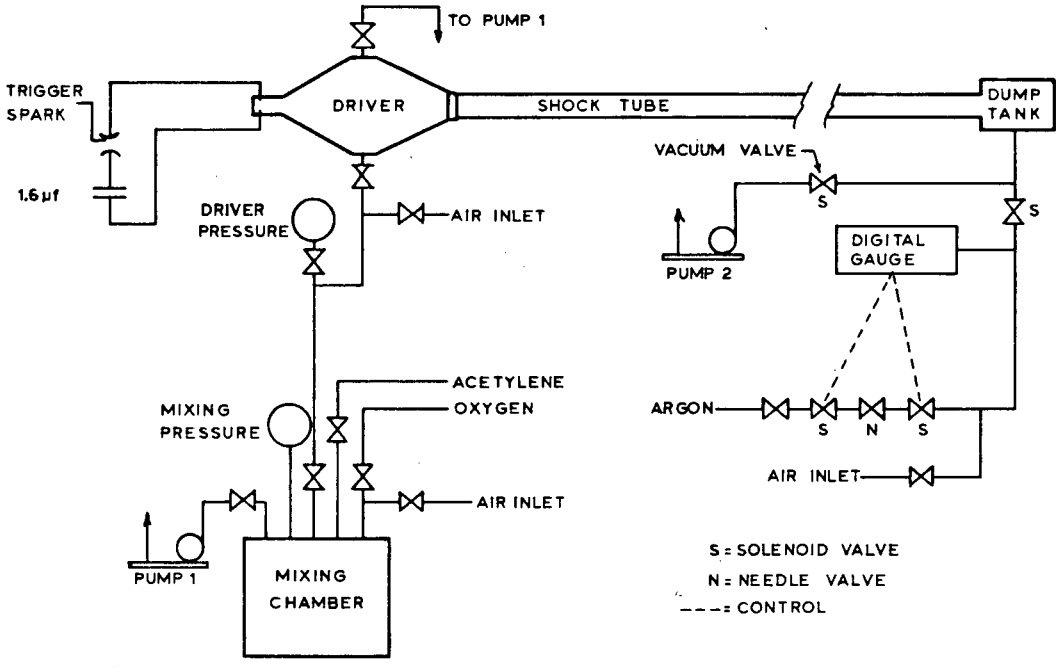

Figure 3.1 Schematic diagram of the shock tube system.

3.1.2 Driver Section

The main body of the driver consisted of two aluminum cones, the first as the divergent section and the second as the convergent (imploding) section (see Figure 3.2). The cones were cast from B 135 aluminum and then machined. They were mated at their bases by a machined aluminum ring to which they were held with flanges. The ring also provided for filling and pumping out the driver through two holes on opposite sides. The total volume of the driver was approximately four litres.

At the back end of the driver a spark igniter housed in lucite was bolted to the first aluminum cone. A spark between these two electrodes initiated the detonation in the driver gas. At the front end of the driver a brass round to square transition piece (one inch long) was bolted to the second aluminum cone. This served to match the round geometry of the driver section to the square cross section of the shock tube itself. Throughout the driver section O-rings were used as vacuum seals. The entire driver section was fastened with steel straps and bolts to its own table which was loaded with 70 Kg of concrete, to decrease the recoil.

The acetate diaphragm was mounted between two O-rings; one on the face of the brass transition piece and the other on a replaceable lucite flange. Both the diaphragm and flange were held in place by the four bolts which bolted the first length of shock tube to the driver (see Figure 3.3). The

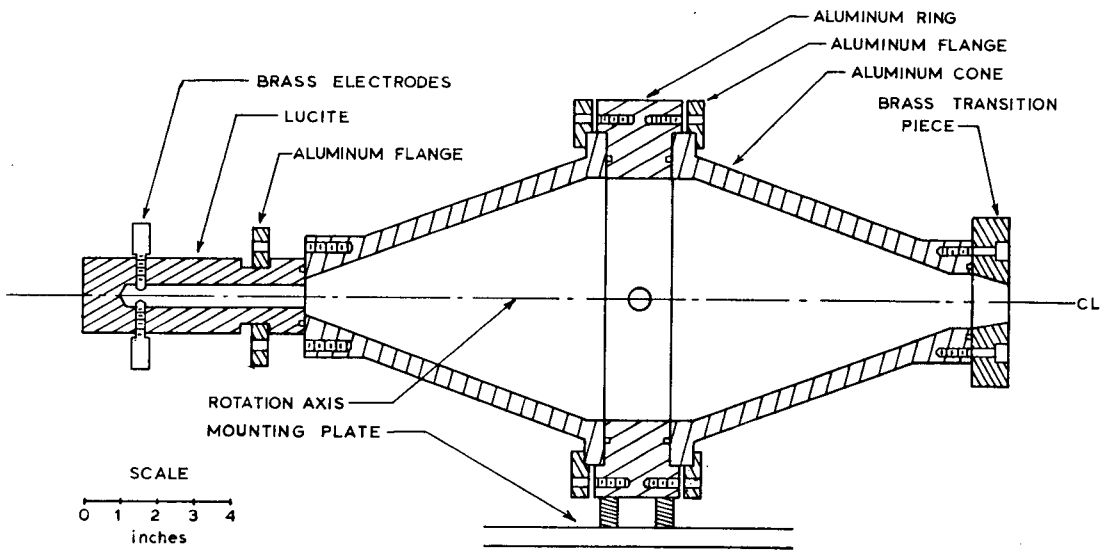

Figure 3.2 Cross section of the driver

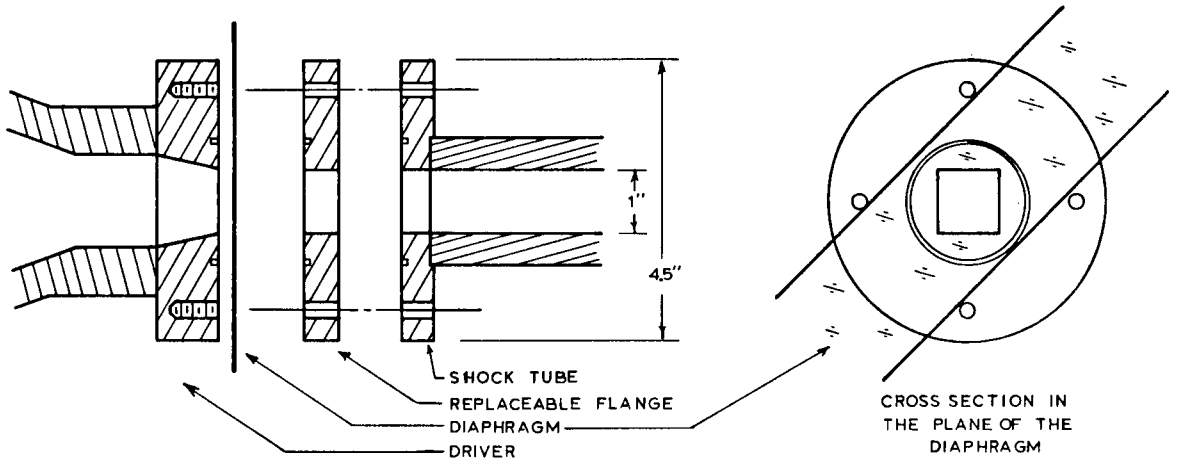

Figure 3.3 Detail of the acetate diaphragm

lucite flange needed replacement occasionally because of erosion caused by the bursting of the diaphragm.

3.1.3 Ignition System

The detonation mixture in the driver section was ignited by a spark between two electrodes. These electrodes were mounted in a short lucite tube at the end of the driver opposite the diaphragm as shown in Figure 3.2. Energy for the spark was stored in a 1.6μf capacitor which was charged to 11 KV (approximately 100J). A triggerable spark gap between the capacitor and the electrodes allowed the shock tube to be fired. This system is shown schematically in Figure 3.1.

3.1.4 Shock Tube

The shock tube itself was built in three interchangeable lengths, which were 50, 75, and 100 cm. long. Flanges and O-ring seals at the end of each section allowed them to be connected together. Each section was made of lucite in a box construction with walls about one half inch thick. The sections were glued together with machine screws every two and one half inches for support.

To make the system rigid the whole shock tube was mounted on a length of aluminum channel. It was supported above the channel on stands which allowed easy access to all sides of the tube. A dump tank of about one litre volume was connected

to the last section of the shock tube.

Periodic cleaning of the shock tube was done by dismantling the sections and cleaning each one with a rectangular swab. A felt cloth soaked in Brasso was mounted on the swab to polish the tube walls.

3.1.5 Pumping And Filling Systems

The oxy-acetylene with which the driver was filled was premixed in a mixing chamber which held enough gas for several shots. This chamber, which stood adjacent to the driver section, was cylindrical in shape and was enclosed in a wire mesh screen for safety. The bottom of the mixing chamber was soldered to the mixing chamber with soft solder so that if the mixture accidentally ignited the bottom would fail first. The oxy-acetylene was mixed two parts oxygen to one part acetylene by pressure. The pressures were monitored on the mixing chamber pressure gauge as each gas was added. Since the mixing chamber was built as a vacuum tank, the total fill pressure never exceeded one atmosphere. After allowing some time for mixing, the driver was filled to the chosen pressure (from 100 to 300 Torr) as shown by the driver pressure gauge. Before a shot was fired isolation valves at the inlet and outlet ports of the driver were closed to protect all gauges and tubing. After a shot the driver was pumped out through a port opposite the filling port.

The shock tube could be either filled or pumped out

through a port in the dump tank. The filling of the tube with the test gas (argon in this case) was controlled by a set point pressure gauge and a solenoid valve. This allowed the tube to be automatically filled to an accurately known pressure. During a shot the pressure gauge was protected with an isolation valve. A rotary pump was once again used to pump out the tube after each shot.

3.1.6 Test Section

In order to make the best use of the shock tube a short test section was constructed as shown in Figure 3.4 and Figure 3.5. It could be bolted between any two sections of the shock tube and thus mounted at a variety of distances from the diaphragm. By using a test section models such as bow shock generators or instrumentation could be mounted in the tube without altering the shock tube sections themselves. The test section had two removeable lids (one top and one bottom) as shown in Figure 3.4 on which the models or instrumentation could be mounted. The lids were of simple design and new ones could quickly be machined if replacements or extras were needed. The test section was built from three quarter inch lucite with O-rings to seal the lids. The lids were clamped together from the outside so that with the O-rings fully compressed the inside faces of the lids were flush with the tube walls (see Figure 3.5).

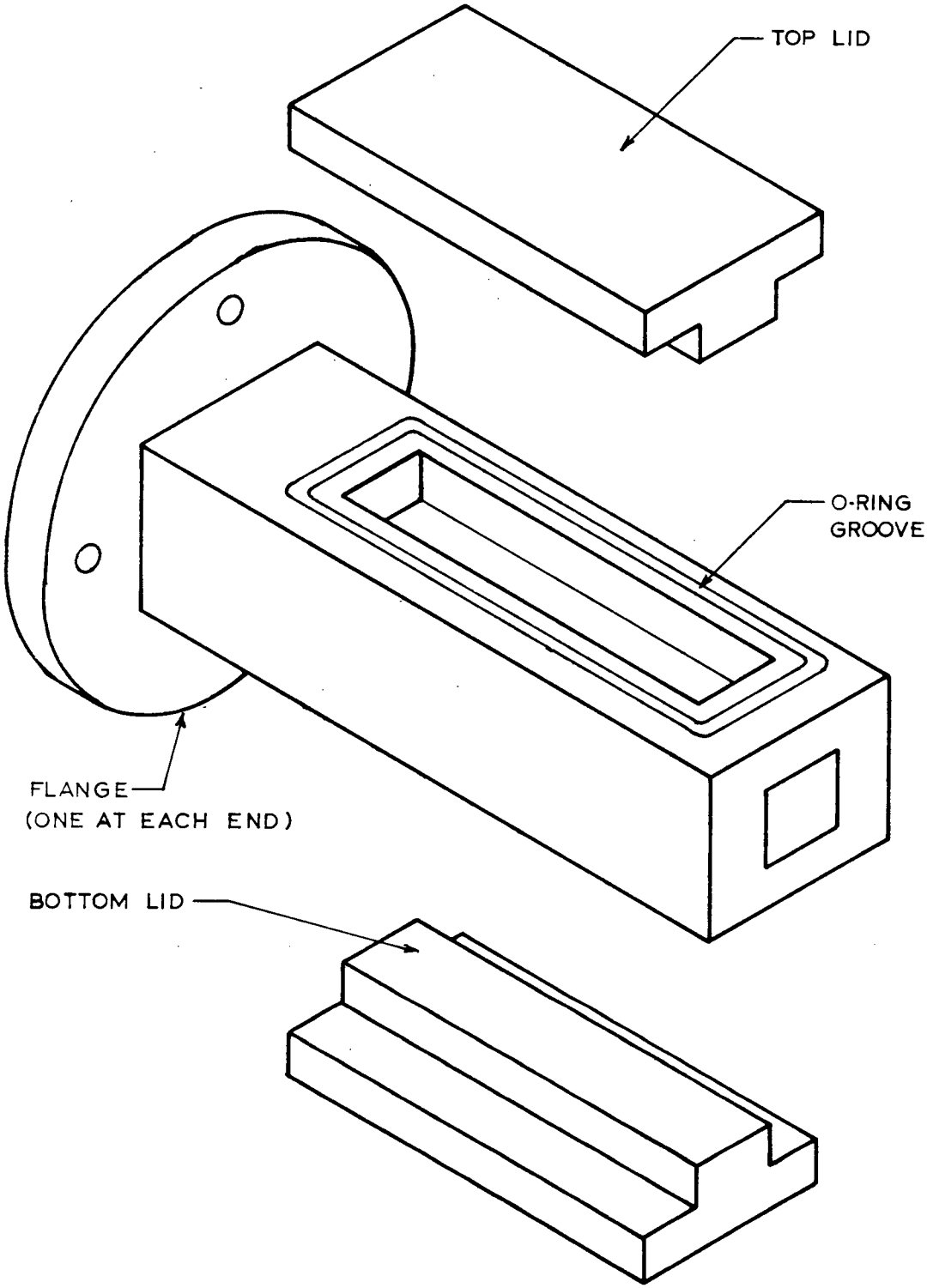

Figure 3.4 The test section with removable lids

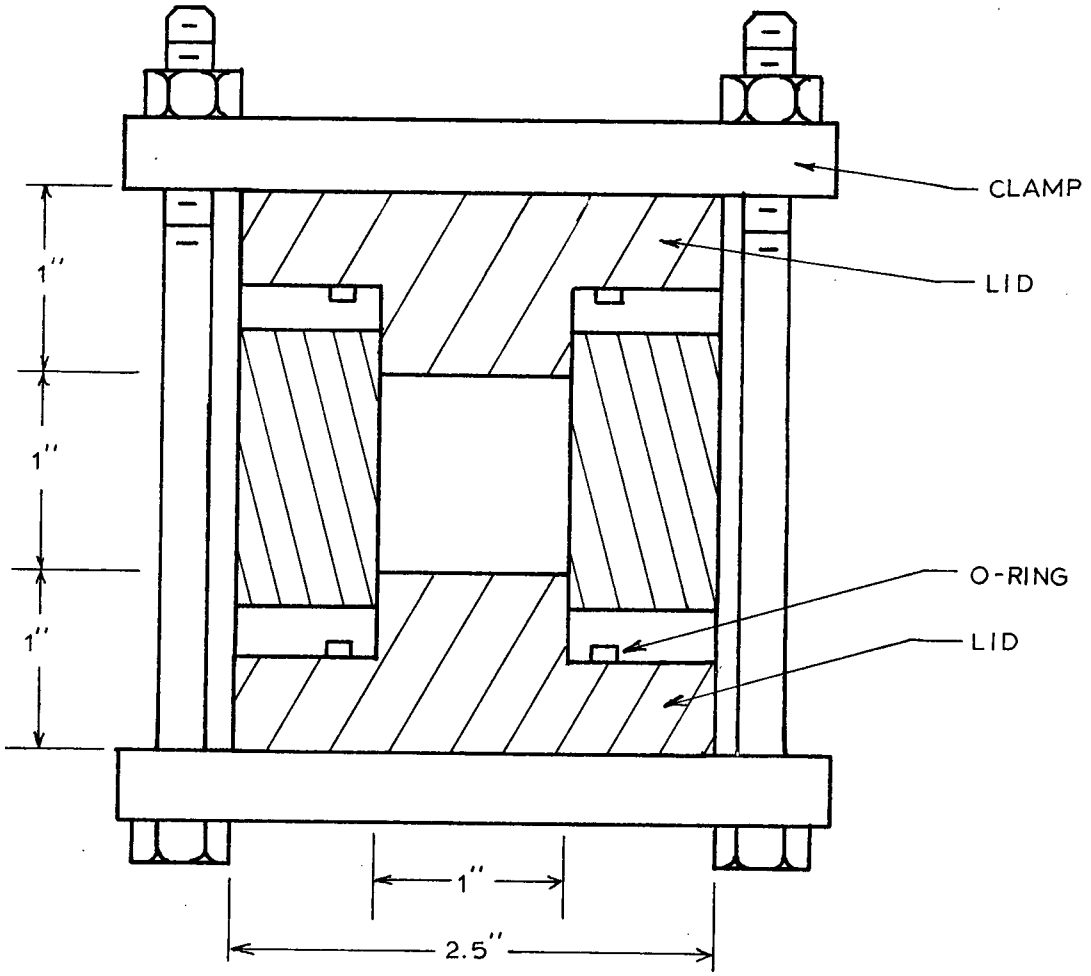

Figure 3.5 Cross section of the test section

3.1.7 Pressure Probe Flanges

Two flanges, each one inch thick, were machined to accomodate piezo-electric pressure probes (see Figure 3.6).

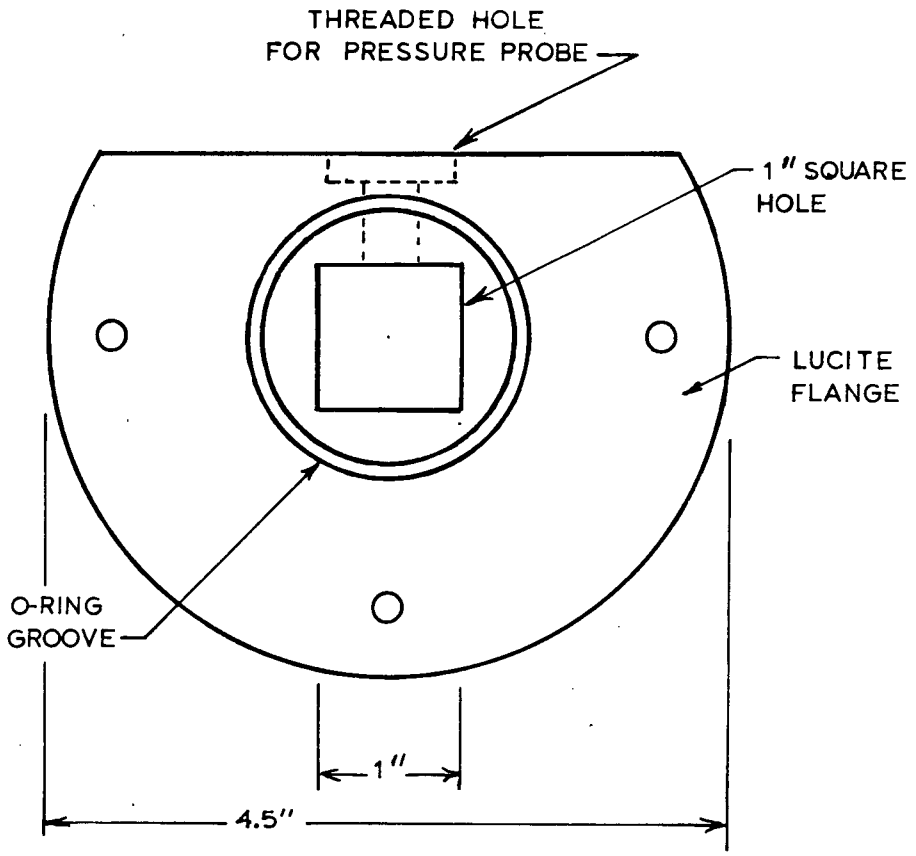

Figure 3.6 The pressure probe flange

These flanges could then be clamped between any of the sections of the tube and used for triggering other apparatus or in a pair at each end of the test section to monitor shock speed. The piezo probes used in this experiment were

manufactured by Celesco Transducer Products Inc. and were type LD25. They had a sensitivity of about .15V/psi. With these probes a check was kept on the reproducibility of the shock speed throughout the bow shock generator test experiments. For the measurement of shock velocities the piezo probe outputs were first buffered through a high input impedance buffer amplifier and then used to trigger a start/stop digital microsecond counter.

3.2 MEASUREMENTS

A number of preliminary experiments were made on the shock tube before the experiments with the bow shock generator were undertaken. The aim of these experiments was to investigate the performance of the shock tube and to investigate some of the properties of the slug of shock compressed argon which travels down the tube. The steadiness of this flow behind the shock was of particular interest. Throughout the experiments a driver gas mixture of one part acetylene to two parts oxygen by pressure was used. The gas used in the low pressure section of the shock tube was always argon.

3.2.1. Dependence Of The Shock Speed On The Fill Gas Pressures

The first set of experiments explored the range of Mach numbers that were available with the shock tube. The shock front speed was measured at a distance of about one metre from the diaphragm for a number of different fill gas pressures. Both the driver pressure and the shock tube pressure were varied. The results are summarized in Figure 3.7 which shows the Mach number measured for each combination of fill gas pressures.

In the case of the driver section, the pressure when the diaphragm bursts, will, of course, be much higher than the driver fill gas pressure. The pressure is increased once behind the detonation wave and once again when the detonation is reflected at the diaphragm end of the driver[17]. No attempt was made to measure this pressure in these experiments but the results from other experiments done in this lab[16] indicate that it is of the order of 100 atmospheres.

In these experiments the speed of the shock was measured with a smear or streak camera. In this technique the axis of the shock tube is imaged onto the slit of the smear camera with a lens. The smear camera records a position versus time history of the luminosity by sweeping the image of the slit across the film. Two markers, spaced an accurate distance apart, were placed on the shock tube wall within the field of view of the smear camera. By measuring the transit time for the shock between the markers on the photograph the shock

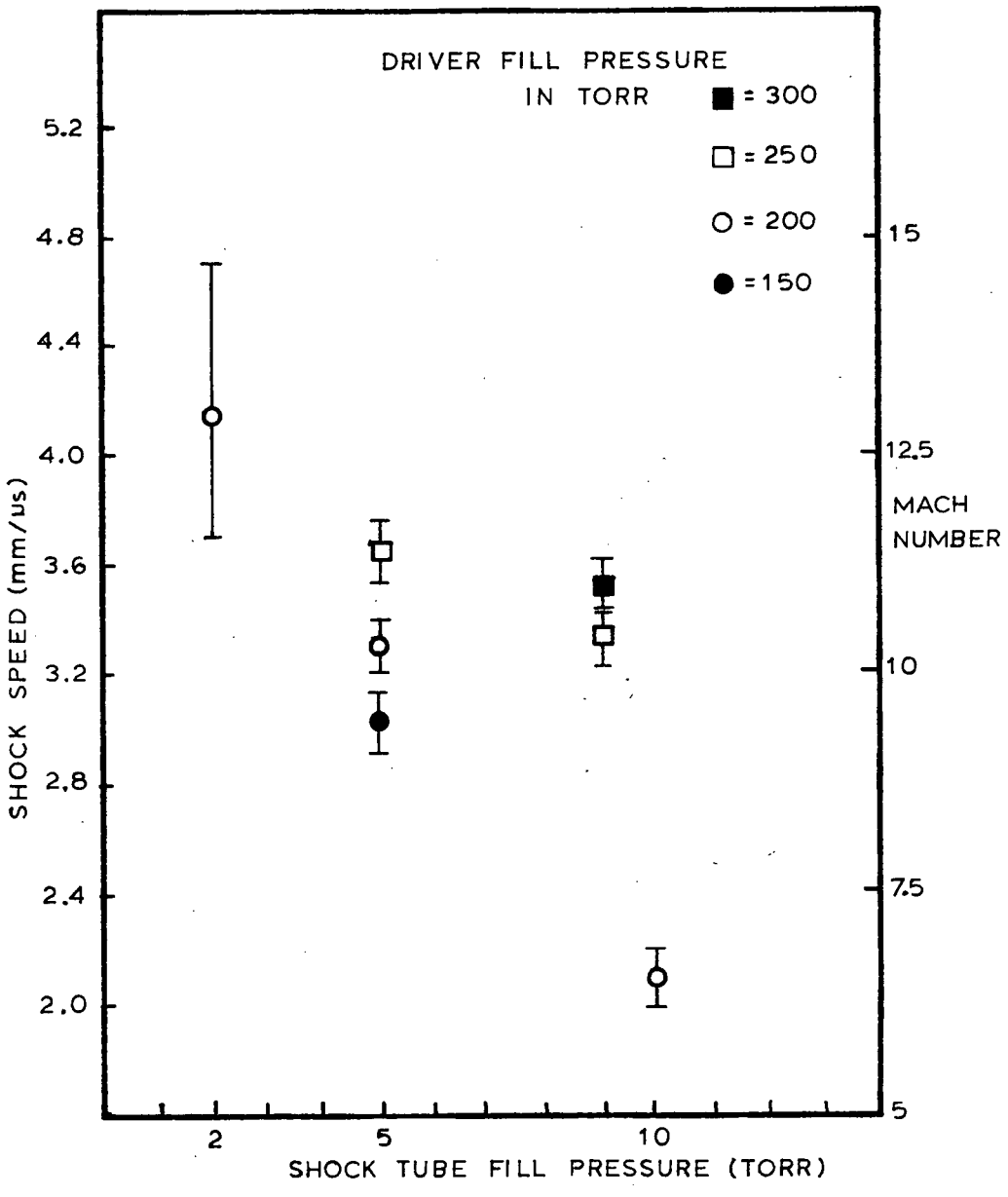

Figure 3.7 The shock speed measured for various fill gas pressures

speed was calculated. A typical smear camera photograph is shown in Figure 3.8. A few of the values included in this

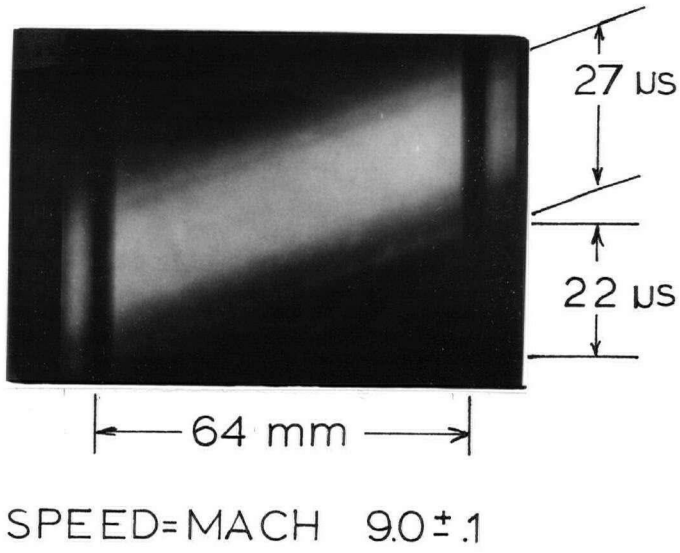

Figure 3.8 A typical smear camera photograph

data were not actually done with a smear camera but rather by measuring the transit time for the shock between two pressure probes as described in the next section.

The results of these investigations show, that in this

shock tube, the Mach number of the shock can easily be varied over a fairly wide range from Mach 6 to Mach 12.5. It can be seen that the design criterion of a Mach 10 to 11 shock propagating into 5 Torr argon was readily achieved.

3.2.2 Dependence Of The Shock Speed On Position

Once the dependence of the shock speed on the fill gas pressure had been established at one position in the tube the variation of shock speed along the tube was investigated. This was done by measuring the shock speed at a number of stations along the tube. These tests were all carried out with a driver fill pressure of 200 Torr and a shock tube fill pressure of 5 Torr.

To measure the shock speed two of the piezo-electric pressure probes were mounted a known distance apart in one of the lids of the test section. The outputs from the pressure probes were put through a high input impedance buffer amplifier and displayed on a dual trace oscilloscope. A third pressure probe mounted immediately ahead of the test section was used to trigger the scope. From the time interval between the rising edges of the two signals and the known distance between the probes the shock speed was calculated. A typical example of the two pressure signals is shown in Figure 3.9.

The shock speed was measured at a variety of distances from the diaphragm by locating the test section between different sections of the shock tube. The results from these

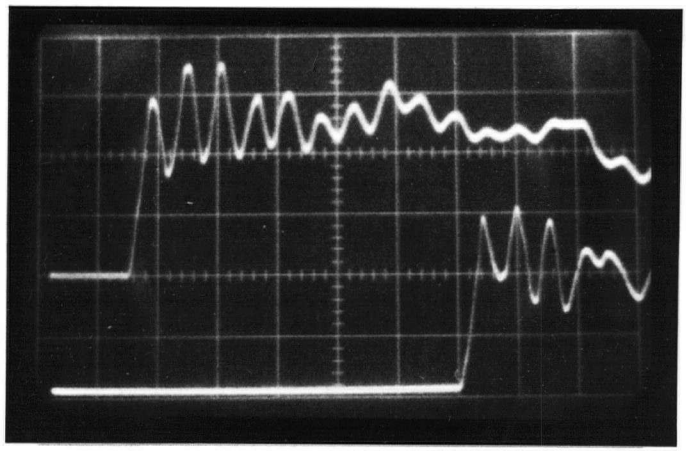

5μs/div
1.0 V/div
PROBE SEPARATION = 102 mm
SPEED = MACH 11.3

Figure 3.9 A typical pair of pressure signals used for shock speed measurement

experiments are shown in Figure 3.10 as a plot of shock speed versus distance from the diaphragm. Each data point is an average from several shots done at that distance. The variation of the speed at any point from shot to shot was quite small, except at a distance of 65 cm. from the diaphragm, where there was as much as a 20 per cent variation.

Figure 3.10 also shows typical pressure signals from several of the stations along the tube. These were obtained with one of the probes in the test section using a long time scale. It was found that the type LD25 probes were best suited for measuring the time of arrival of shocks or

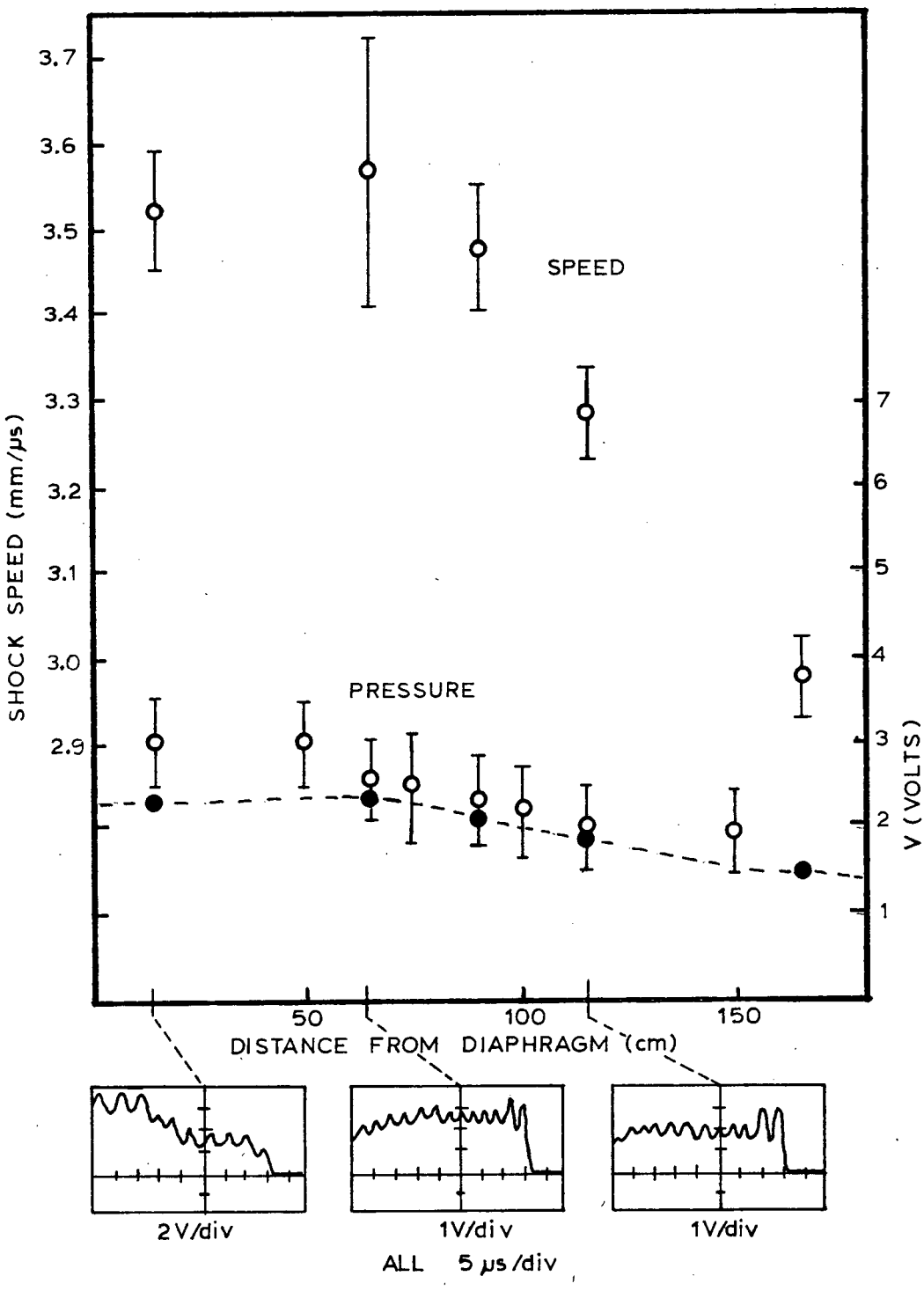

Figure 3.10 Shock speed as a function of distance from the diaphragm. The magnitude of the pressure probe signal immediately behind the shock (V) is shown. The dotted line is the theoretical value of V calculated from the shock speed. Representative pressure probe signals from three locations along the tube are also shown

observing strong pressure gradients in the flow. Distributed rarefaction waves or short regions of constant pressure were hard to identify because of the ringing of the probe signal. The pressure step across the shock front was fairly well defined however, and this jump, in volts, is shown for several stations along the tube in Figure 3.10. This gives an indication of the relative strength of the shock as a function of the distance from the diaphragm.

The results show one rather interesting feature. A slight increase in shock speed is observed about 65 cm. from the diaphragm. After this the shock decays fairly uniformly for the next metre. This increased speed is consistent with the pressure trace shown from the previous station as shown in Figure 3.10. It appears that due to some unsteadiness in the driver a compression wave is emitted from the driver some 30 microseconds after the shock has been launched. This compression wave catches up to and reinforces the shock about 65 cm. from the diaphragm accounting for the increased speed measured in that region. If in some shots the compression wave were to catch the shock just before 65 cm. and in other shots not until just after 65 cm. there should be a large shot to shot variation in the measured speed. This large scatter in velocities was indeed observed at a distance of 65 cm. from the diaphragm.

3.2.3 The X-T Diagram For The Shock Front

In addition to being used to measure shock velocities the pressure probes were used to measure the absolute time of arrival of the shock at each station along the tube. The arrival time was measured from the time the detonating spark in the driver section was triggered. These results are shown in Figure 3.11. From other experiments it is known that the detonation arrives at the diaphragm approximately 250 microseconds after the spark. The delay before the diaphragm bursts can therefore be seen to be of the order of 25 microseconds.

These results show the same essential features as the velocity measurements. At about 65 cm. from the diaphragm there is the same increase in speed noted as in the previous measurements. This is followed by a fairly uniform decay in shock speed from this point onward.

For reference, the theoretical position of the contact surface has also been shown in Figure 3.11. The position of the contact surface was calculated from the compression ratio across the shock at each point.

3.2.4 Smear Camera Measurements

The smear camera photographs, from which the velocities were measured, also yield some information about the duration and homogeneity of the flow behind the shock. The luminosity of the shock front itself is often very faint, as can be seen,

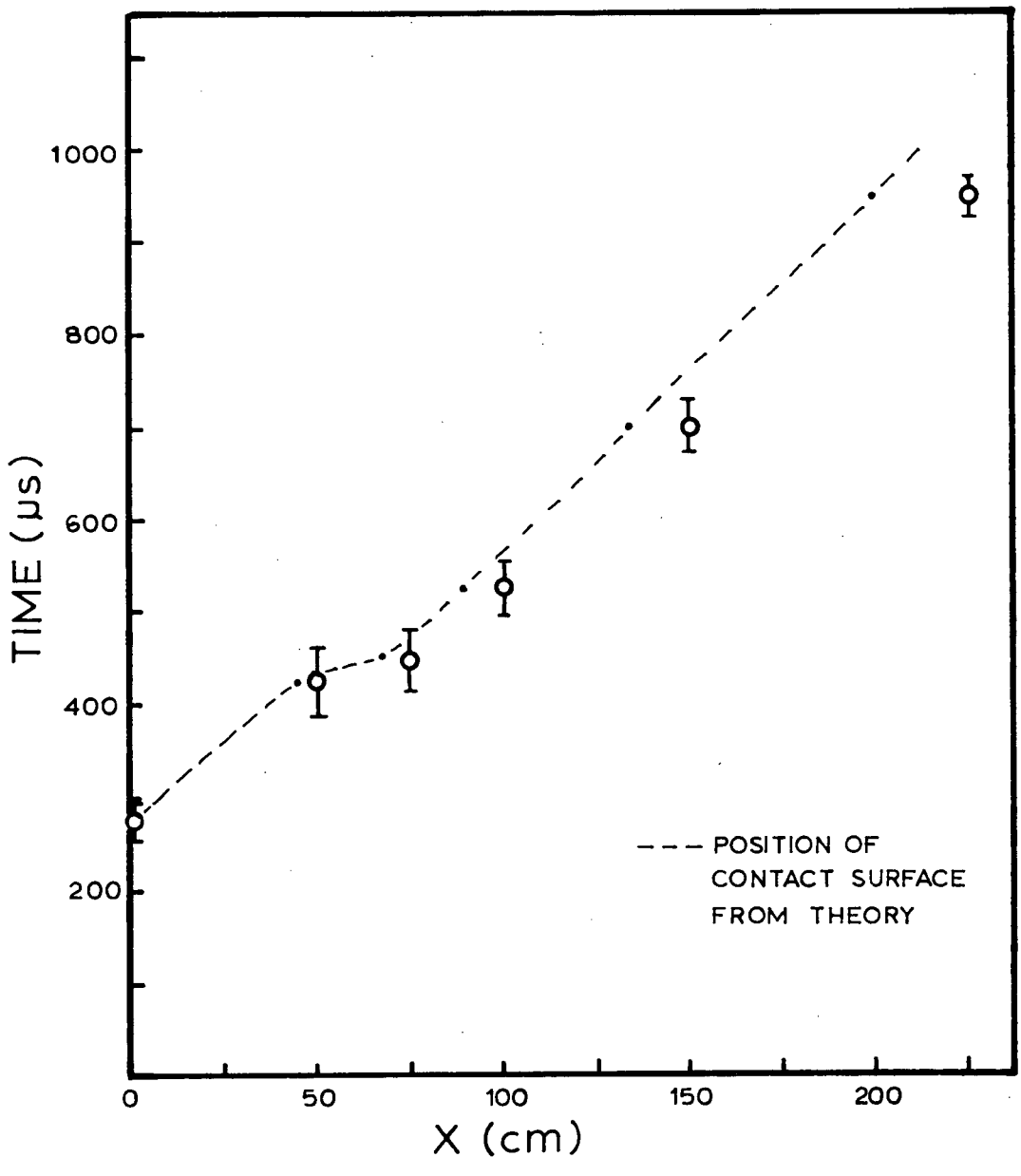

Figure 3.11 The X-T diagram for the shock wave

for example, in Figure 3.8. It was necessary therefore to ensure that the faint luminosity in these photographs was in fact the shock. To check that the shock had been properly identified several experiments were done with the arrangement shown in Figure 3.12. A pressure probe was mounted in the

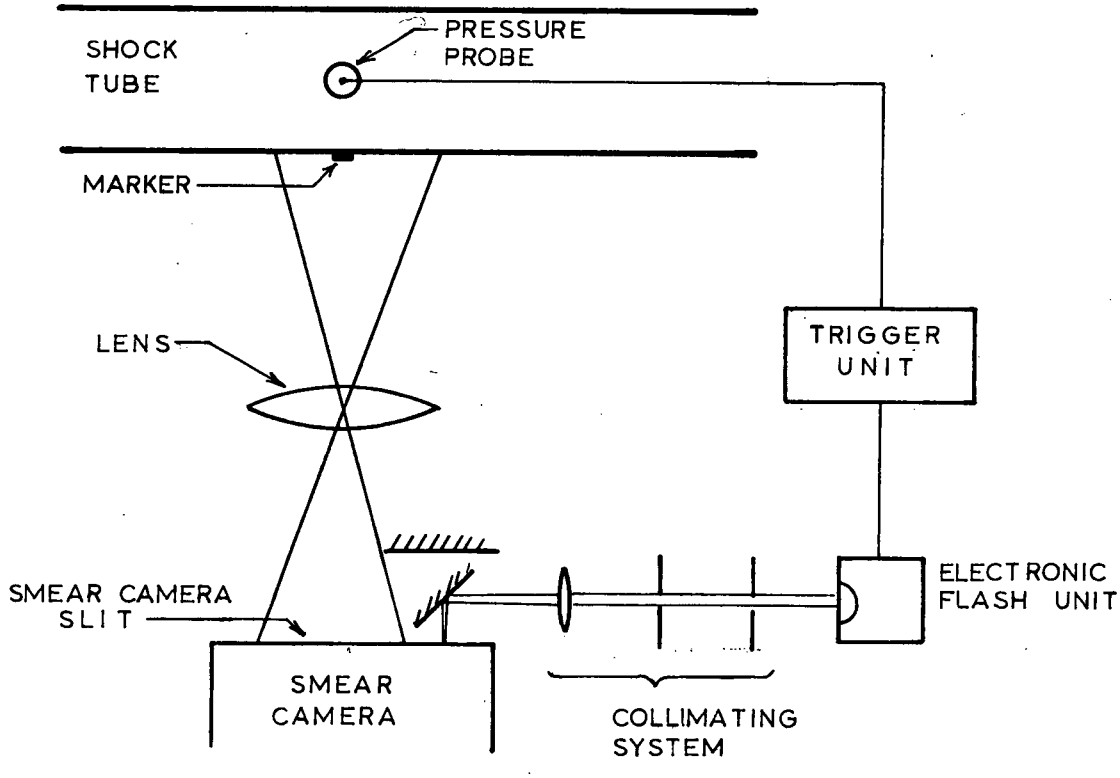

Figure 3.12 The apparatus used to check the interpretation of the smear camera photographs

centre of the field of view of the smear camera and its position was marked in the pictures by placing a black band on

the shock tube. The signal from the probe was used to trigger an electronic flash unit that was focused onto the slit of the smear camera near one end. Figure 3.13 shows one of the smear

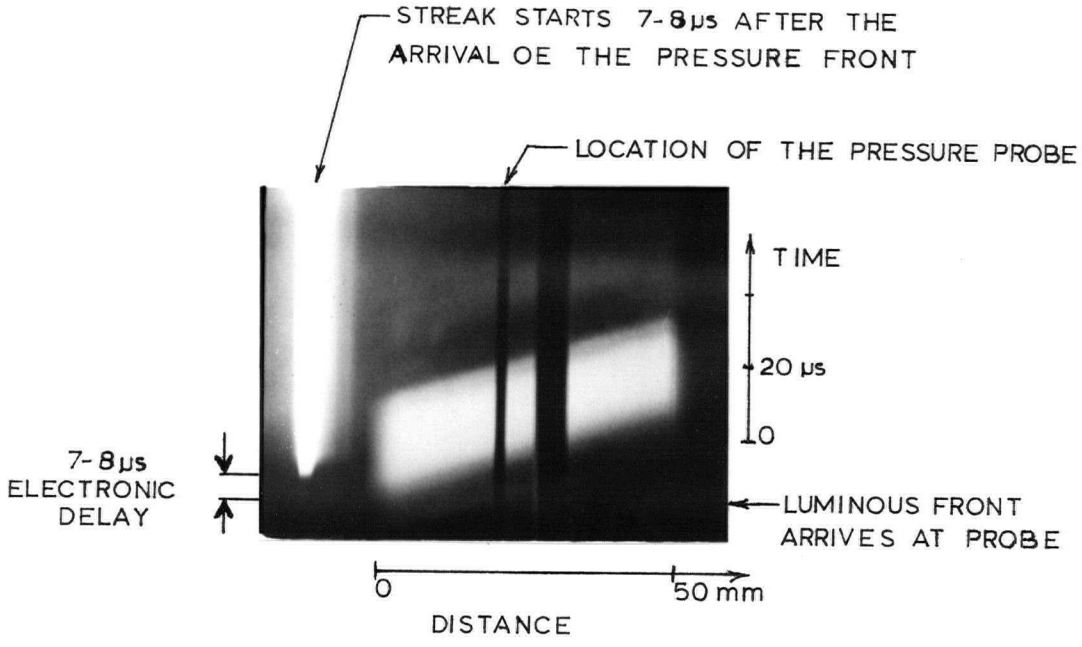

Figure 3.13 A typical smear camera photograph used to check that the first faint luminosity was the shock

camera photographs taken in this way. The start of the flash gun streak, minus a predetermined 7-8 microsecond electronic delay, marks the point in time that the pressure shock arrives at the probe. This time can be seen to correspond very well with the time of arrival of the faint luminosity at the

pressure probe.

An examination of the smear camera photographs showed that the luminosity of the gas behind the shock was neither uniform nor completely reproducible from shot to shot. Figure 3.14 shows two photodensitometer tracings that were taken from

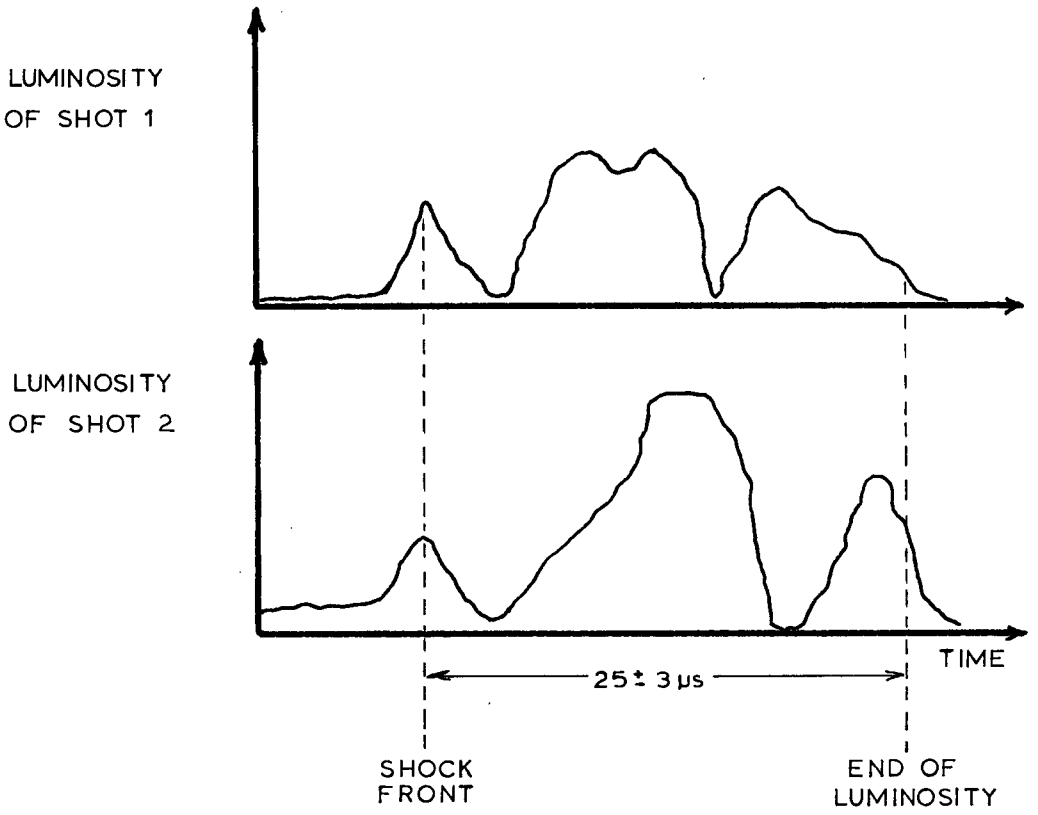

Figure 3.14 Photodensitometer records of two smear camera photographs for identical initial conditions

smear camera photographs of two shots fired with identical initial conditions. This shot to shot variation is probably due to small velocity variations which translate into larger variations in electronic excitation in this temperature region. Despite this shot to shot variation experiments done later on the bow shock generators showed how to interpret these photographs consistently. It was found that the useful test flow ended at a time corresponding to the last sharp drop in the luminosity (see Chapter 5.1). For all the smear camera photographs, the total time from the arrival of this drop, was measured to be fairly constant.

3.2.5 Test Time

All the information from the smear camera photographs and pressure probe tracings was combined to determine the test time. At any point in the shock tube this test time starts when the shock arrives and in theory would last until the arrival of the contact surface. In these experiments the flow behind the shock is only useful for as long as it is ionized and supersonic.

On the smear camera pictures the test time was estimated from the duration of the luminosity, as was discussed in section 3.4. From the pressure probe signals the test time was taken to be the duration of the "constant" pressure region following the shock. A theoretical value for test time, the time interval between the shock and the contact surface, was

also calculated. Using each of these methods an estimate of the test time was made at a number of stations along the tube. The results are shown in Figure 3.15 as a plot of the test time estimated versus position along the tube.

3.3 SUMMARY

Based on the experiments done with the shock tube it was decided to conduct the bow shock generator tests at a distance of about 90 cm. from the diaphragm. At this point the velocity was relatively constant from shot to shot and the Mach number was still quite high. Both the smear camera and pressure probe results indicated that there should be at least 25 microseconds of test time after the arrival of the shock. Some shot to shot variation of the conditions in the flow behind the shock might be expected, however, as is evidenced by the smear camera photographs.

It might have been possible to achieve a slightly longer test time by moving somewhat further from the diaphragm. However, because of discrepancies in the data from the stations there, it was decided to test the generators at a position 90 cm. from the diaphragm. One 75 cm long section of the shock tube was therefore interposed between the diaphragm and the test section so that the bow shock generators would be located about 90 cm downstream of the diaphragm.

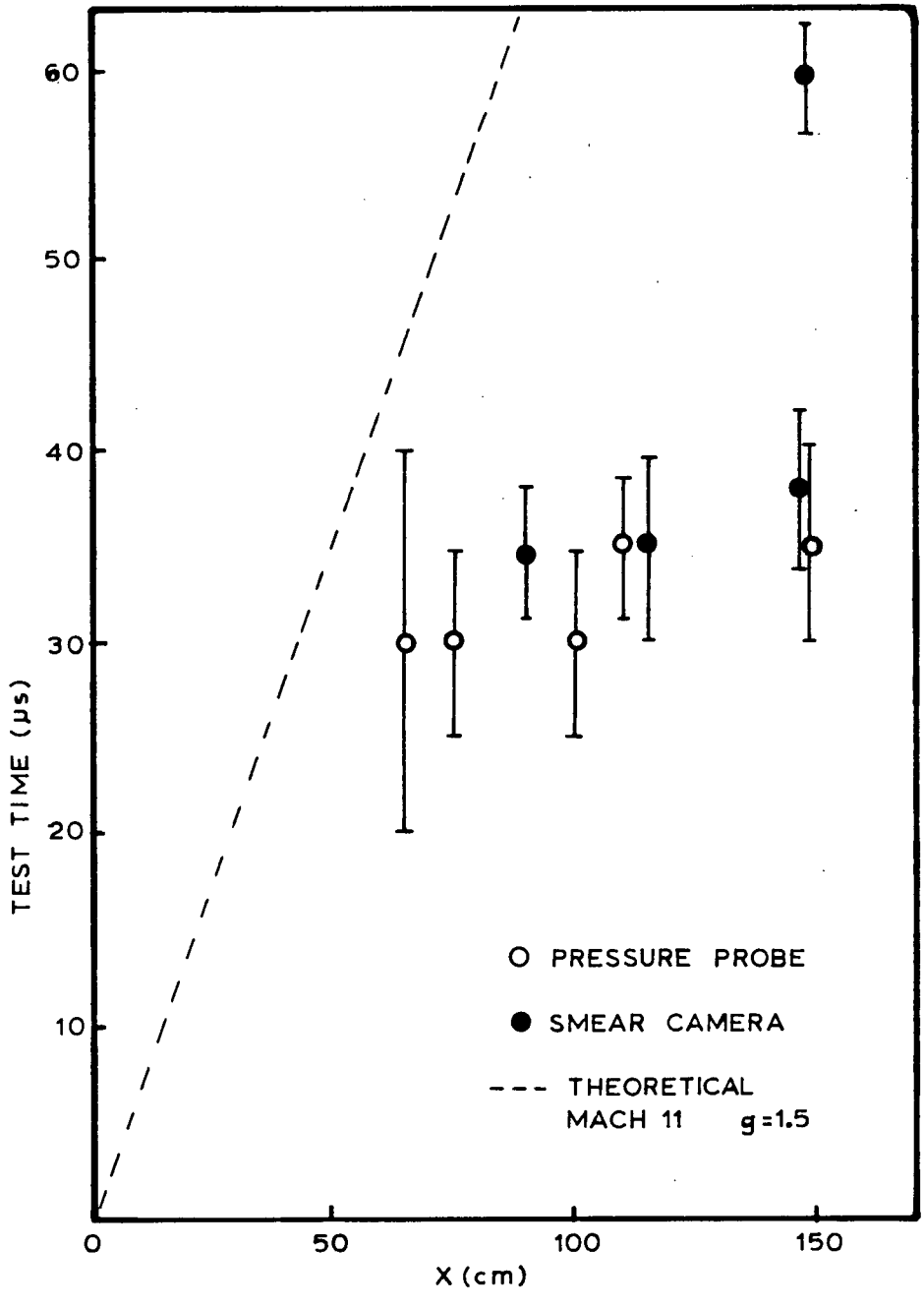

Figure 3.15 Test time as a function of position in the shock tube

CHAPTER 4. CONSTRUCTION OF GENERATOR TEST SYSTEMS

As outlined in the introduction, two different configurations had been suggested for increasing the current or voltage output of bow shock generators by using several shocks. To test these concepts two different generator systems were built.

One system was designed to investigate the power extraction from several shocks which stood physically in parallel across the flow. The other system was designed to investigate the power extraction from a number of shocks formed by successive reflections from the walls.

In each case the systems were built so that they could be mounted on the test section lids. The wedges and mounting struts for the generators were made to be as thin as possible, to minimize the obstruction of the flow in the shock tube.

4.1 PARALLEL SHOCK GENERATORS

In this configuration a number of shocks, created by a number of wedges, stood physically in parallel across the flow as shown schematically in figure 4.1.

Two electrodes were mounted on each wedge, with seperate electrical leads, so that power could be extracted from each shock seperately. The outputs from the generators could then

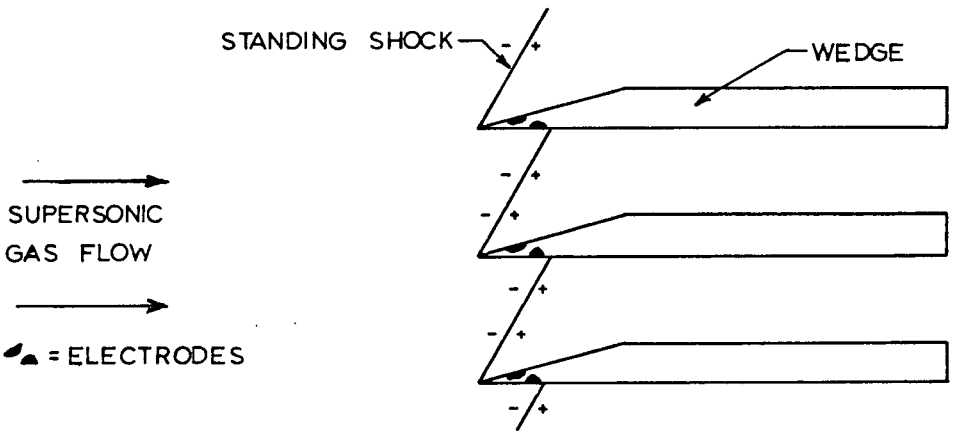

Figure 4.1 Schematic diagram (cross section) of the parallel shock generators

be connected electrically in parallel or in series as desired for testing. So that the electrodes would not be influenced by the potential elsewhere in the plasma the rest of the wedge, or its surface at least, had to be made of insulating material.

Due to the space limitations in the shock tube, only two standing shocks, created by two wedges were investigated. Figure 4.2 shows a drawing of the generator system used to test parallel and series connections of parallel standing shocks.

The main body of the wedge was built of an insulating material. The insulator was required to withstand high temperatures, be machineable, and have good mechanical strength. The asymmetric shape of the wedges used in this part of the experiment meant that the noses of the wedges experienced considerable bending moments and thus mechanical strength was crucial. A number of insulators were tried for

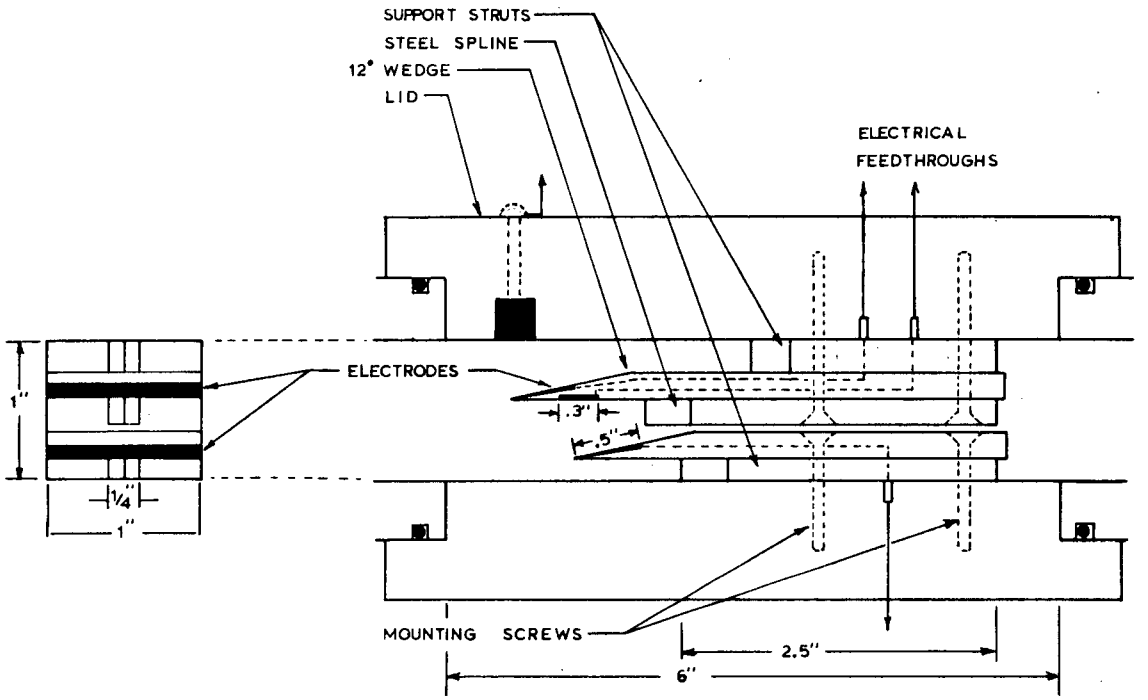

Figure 4.2 A cross section of the parallel standing shock generating system.

this purpose, but a phenolic resin board was found to be most satisfactory. Machineable ceramics were also considered, but they were judged to be too brittle and weak for this application. In practice it was found necessary to reinforce the upper wedge with a steel spline as shown in figure 4.2.

A number of materials were tried for use in electrodes, but steel was found to be most practical in terms of durability. Steel was therefore used as an electrode material throughout. The top (front) electrodes on the tip of both wedges were subjected to such damage, probably due to debris from the ruptured membrane, that it was found necessary to heat treat (case harden) them after machining. After heat treating the electrodes were glued, with epoxy, into slots milled in the wedge.

The bottom electrode on the upper wedge must be completely in front of the standing shock produced by the lower wedge, otherwise the electrode will short out the potential across the lower shock. Since the wedge angle was quite small (12°) it was very difficult to squeeze in two electrodes and their leads right at the tip of the wedge and still retain sufficient mechanical strength. The bottom electrode of the upper wedge was therefore removed about one half inch from the tip and the whole upper wedge moved forward to keep the electrode clear of the lower shock (see figure 4.2). Staggering the wedges like this made design and construction easier but it did shorten the test time slightly

since both wedges were not always in the supersonic flow at the same time.

In the first experiments the wedges were mounted with small machine screws through the walls of the test section. However because the wedges were thin, they tended to fracture around the mounting holes. In later experiments the wedges were therefore mounted on support struts from the top and bottom lids (see figure 4.2). These support struts were also built from phenolic resin board. Mounting the wedges on struts from the lids was not only found to be stronger, but also meant that the wedges could easily be removed for cleaning between shots. Furthermore, the electrical connections to each electrode were easily made by running a wire through the body of the wedge, through the centre of the strut, and out via a connector in the lid.

4.2 REFLECTED SHOCK GENERATORS

In this configuration several standing shocks were created by successive reflections of one shock from the walls, as shown schematically in figure 4.3. By using a number of electrodes mounted on the wall and on the wedge, the output from each shock could be measured separately or the outputs could be connected in series. There were no provisions for parallel connections.

For the flow conditions in the shock tube the standing shock was only reflected from the wall once before it became

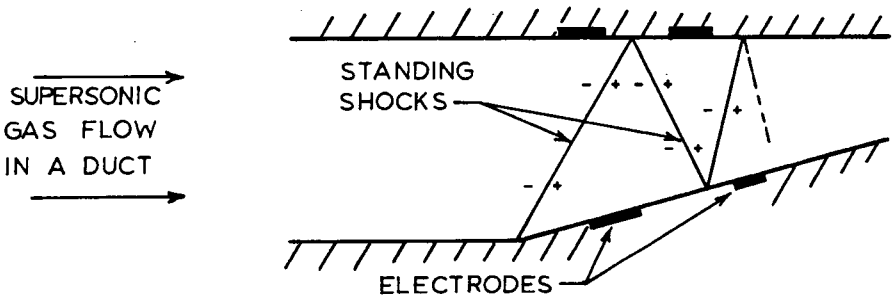

Figure 4.3 Schematic diagram of the reflected shock configuration

very weak. After this point the flow was nearly sonic. Figure 4.4 shows a drawing of the generator system used to investigate the power output of a standing shock and its first reflection from the wall.

The construction of this system was considerably simpler than the multiple wedge system. The symmetric shape of the wedge meant that the wedge was not subject to undue bending stress and did not need a steel reinforcing spline. The construction materials were similar to those used in the multiple wedge experiments. The electrodes were all made from steel, while the body of the wedge and the support strut were made from phenolic board. Electrical connections were once again made with a wire led through the body of the wedge and out through the support strut to the lid.

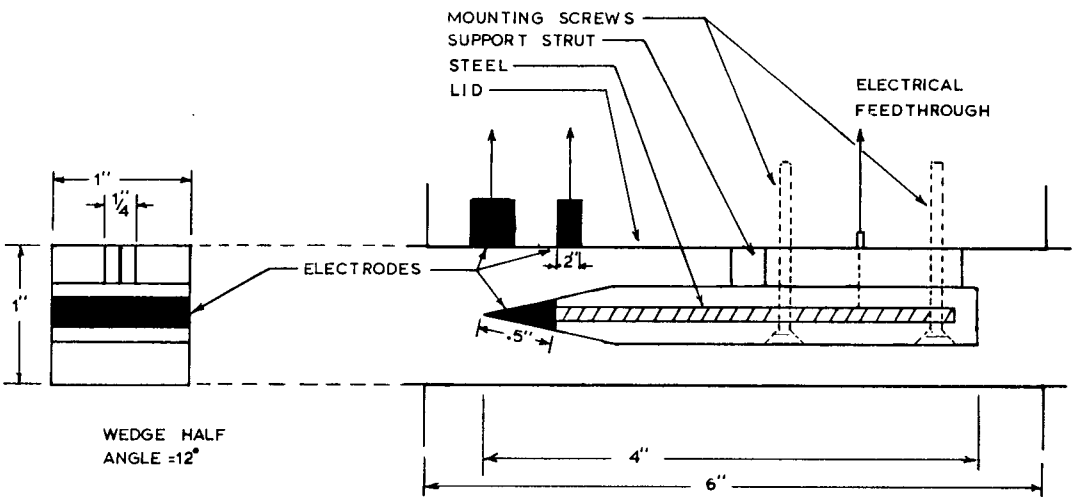

Figure 4.4 A cross section of the reflected shock generator system

4.3 PROVISIONS FOR GENERATOR CONNECTIONS AND POWER MEASUREMENT

For the experiments on either configuration a patch panel was mounted immediately outside the test section so that leads from the electrodes could be connected together in any combination. This allowed the generators to be run individually or connected together in series or in parallel. The panel also had plug-ins for resistors so that each generator or combination could be loaded as desired. The output of the generator into the load was found by measuring the voltage across accurately known load resistors. Differential amplifiers and a dual beam oscilloscope were used for all output voltage measurements.

CHAPTER 5. EXPERIMENTS

Based on the tests done on the shock tube (see chapter 3) it was decided to conduct the bow shock generator tests with the test section located 75 cm. from the diaphragm. This meant that the generators themselves were about 90 cm. from the diaphragm.

The shock tube was operated with an oxy-acetylene fill pressure of 250 Torr and an argon fill pressure of 5 Torr. This gave an incident shock at a speed of 3.6 mm/microsecond (Mach 11.4). From this speed and the shock relations, including the effects of ionization (see Appendix A), the following parameters were calculated for the supersonic flow in the test section, during the test time.

$p_2 = 1.15 \times 10^6$ dynes/cm^2 ≃ 1 Atmosphere

$\rho_2 = 5.3 \times 10^{-5}$ gm/cm^3

$T_2 = 10{,}300$ K

$h_2 = 6.5 \times 10^{10}$ ergs/gm

$u_2 = 2.88 \times 10^5$ cm/sec

$M_2 = 1.58$

$n_{e2} = 2.1 \times 10^{16}$ cm^{-3}

$\alpha_2 = 6.026$

$g_2 = 1.51$

A flange with a pressure probe in it was inserted immediately ahead of the test section. By feeding the pressure pulse from the incident shock through a number of variable delay units, all the instrumentation for the test section could be triggered with very little jitter.

The wedges used in the generators were all machined to have a 12° wedge angle. This allowed comparison of all the results from these experiments, as well as a comparison with other work being conducted in the lab. The choice of the wedge angle was governed by two factors. The angle must be large enough to produce a strong standing shock, but not so large that the shock detaches. If the shock were to detach, the flow parameters behind it could no longer be predicted by plane oblique shock theory. The construction of the wedges has been discussed in more detail in Chapter 4.

It was quickly found that deposits were left on the electrodes after each shot. The deposits appeared to be due, at least in part, to hot debris from the acetate diaphragm carried with the flow. To keep the electrode surfaces as clean and uncontaminated as possible the wedges and electrodes were removed and sanded with fine sandpaper after each shot. They were then cleaned with methanol and replaced in the shock tube which was pumped for at least one half hour before the

next shot was fired.

A consistent numbering system has been adopted for all electrodes in this chapter. They have been numbered from zero to five and the voltage measured between any 2 electrodes will always be designated $V_{AB}=V_A-V_B$.

5.1 INDIVIDUAL SHOCK GENERATOR EXPERIMENTS

The first series of experiments measured the output from a single standing shock, as shown schematically in Figure 5.1.

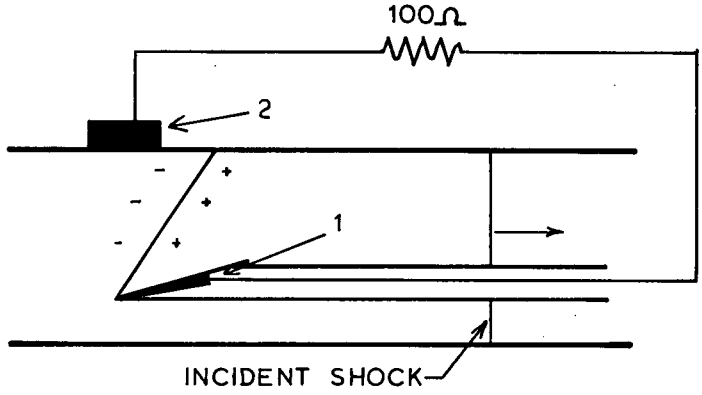

Figure 5.1 Single standing shock generator stretching across the whole tube

The wedge was mounted one quarter inch off the floor of the test section so that it would not be in the boundary layer. The development and stability of the standing shock was monitored with a high speed framing camera. Typical results

of the voltage measured across the shock and an example of the camera pictures are shown in Figure 5.2. The voltage was measured with a 100 Ohm load across the generator. Since the internal resistance of the generator was found to be of the order of a few Ohms the voltage measured across 100 Ohms represents the open circuit voltage for the generator. By using a resistor as small as 100 Ohms spurious signals due to high impedence noise sources were eliminated.

From a comparison of the framing camera pictures and the voltage trace it can be seen that there is an initial transient signal associated with the incident shock. The standing shock is not well established until some 10 - 15 microseconds after the first rise of the voltage, and the signal was considered to be simply a transient up to this point. By the time of the fifth framing camera picture the standing shock is beginning to lose its well defined edge and the voltage becomes unsteady, as shown by the marked increase in the signal. In other cases it was observed that the voltage fell rapidly to zero after this point. The time from the arrival of the shock to the end of the test time can be seen to be about 27 microseconds from both the framing camera pictures and the voltage trace. This correlates very well with the duration of the strong luminosity in the smear camera photographs (see Figure 5.3). These measurements allowed the test time to be predicted from the smear camera photographs as was done in Chapter 3.

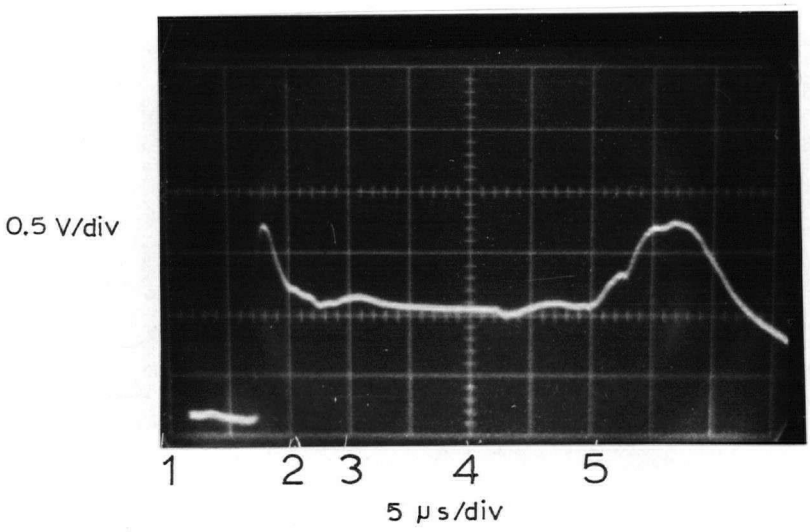

SHOCK VOLTAGE V_{51} (SEE FIG. 5.1)
(ACROSS 100 Ω)

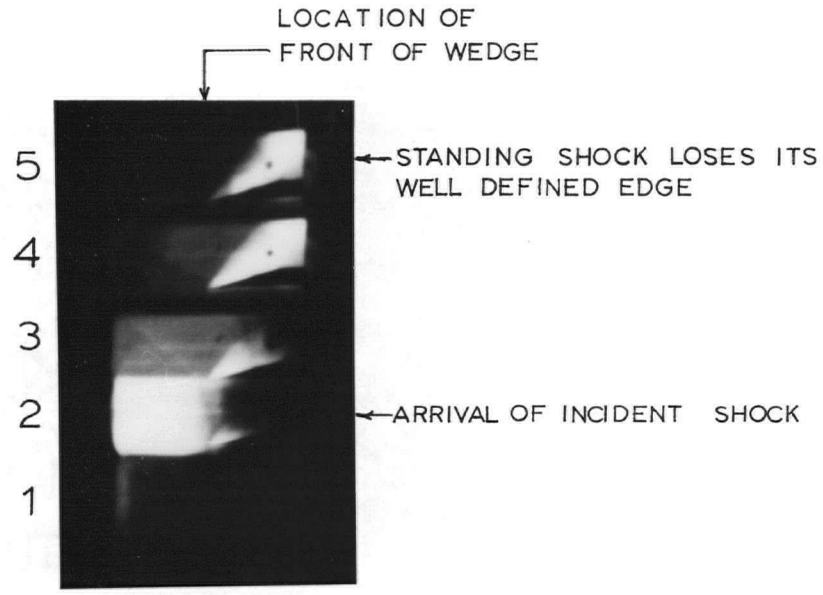

FRAMING CAMERA PHOTOGRAPH
(TIMING SHOWN ABOVE)

Figure 5.2 Single Shock Generator Results

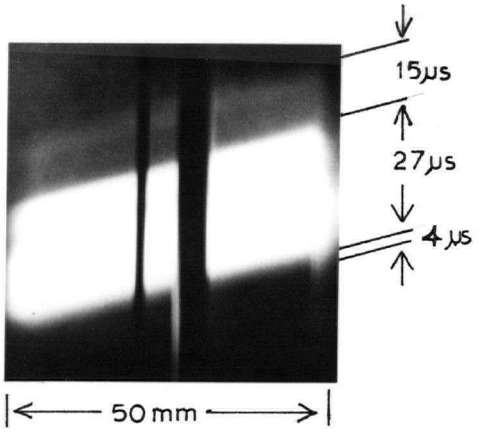

SHOCK SPEED MACH 11.4

Figure 5.3 Smear camera photograph of the slug of test gas taken 90 cm. from the diaphragm.

In order to investigate the output of the generator under load the load resistor was varied from shot to shot so that a V-I characteristic could be plotted for the single shock. The voltages were always read from the oscillograms 15 - 20 microseconds after the rising edge, when the standing shock was well established. The characteristic which is shown in Figure 5.4 indicates the effective internal resistance of the generator is about 5.5±.5 Ohms. The power output of the generator as a function of current is shown in Figure 5.5

The next series of experiments was done with two wedges as shown in Figure 5.6. The output from each shock was measured separately. Typical open circuit voltage signals and a framing camera picture series are shown in Figure 5.7. The

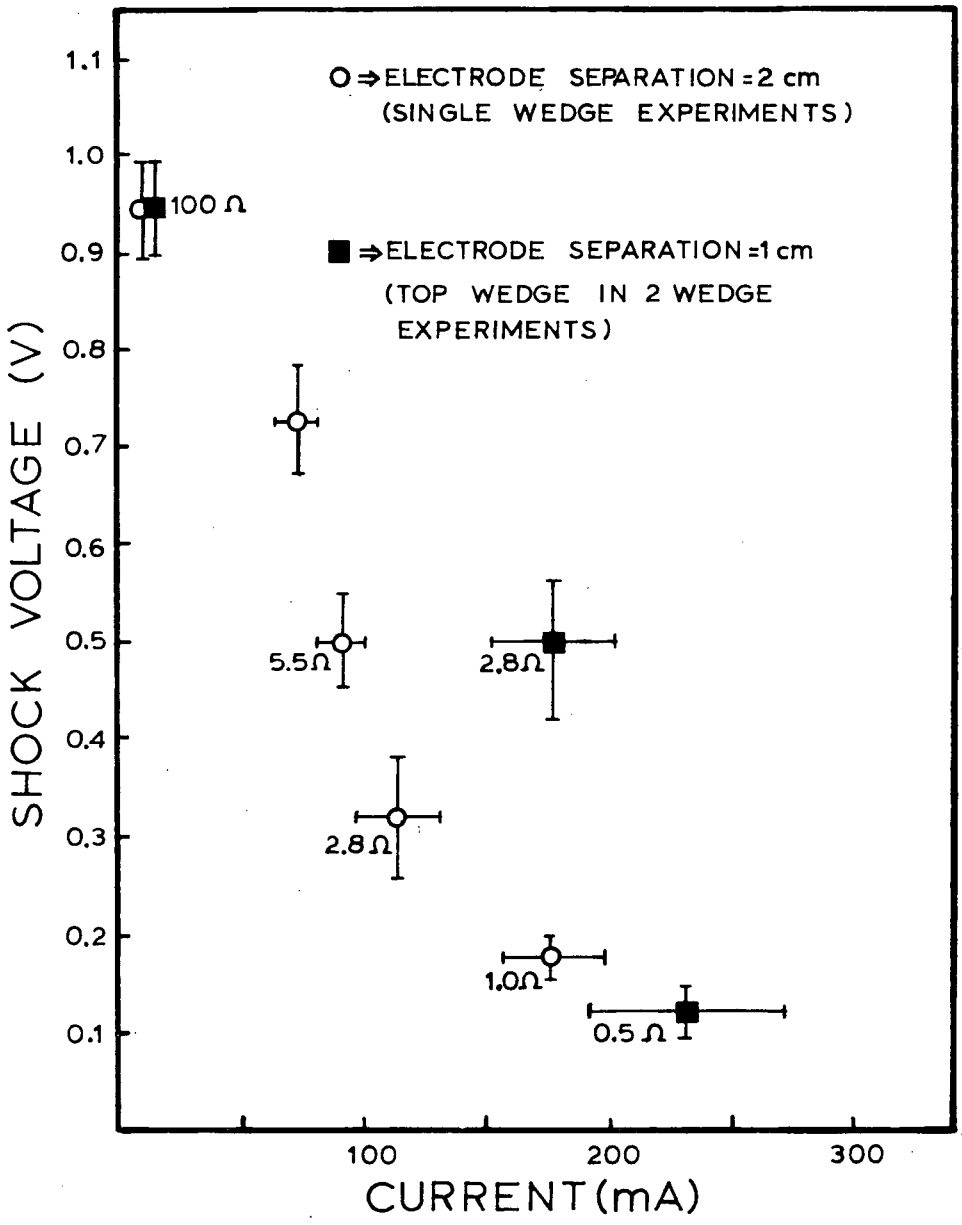

Figure 5.4 V-I characteristic for two individual generators

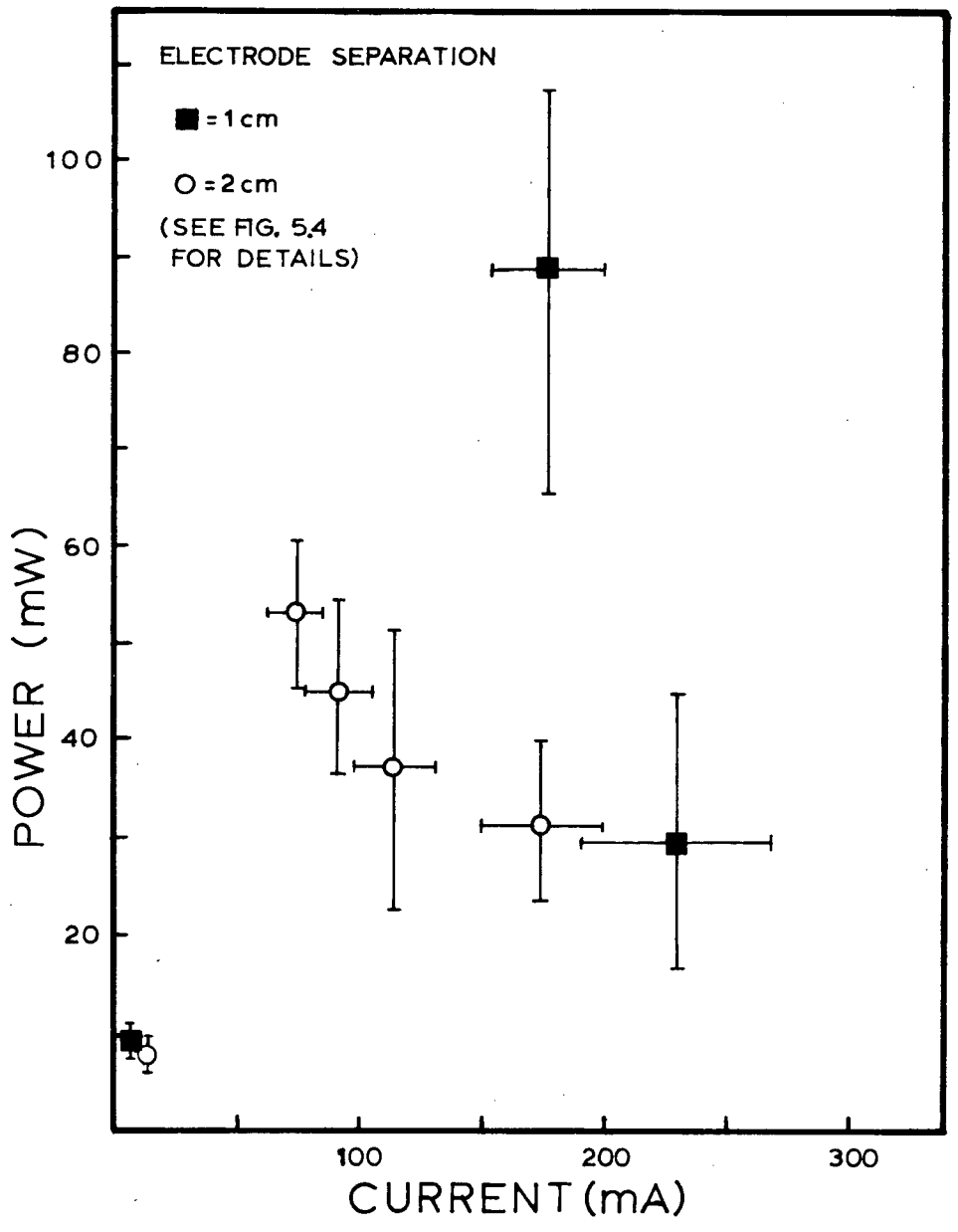

Figure 5.5 Power output vs current for two individual generators

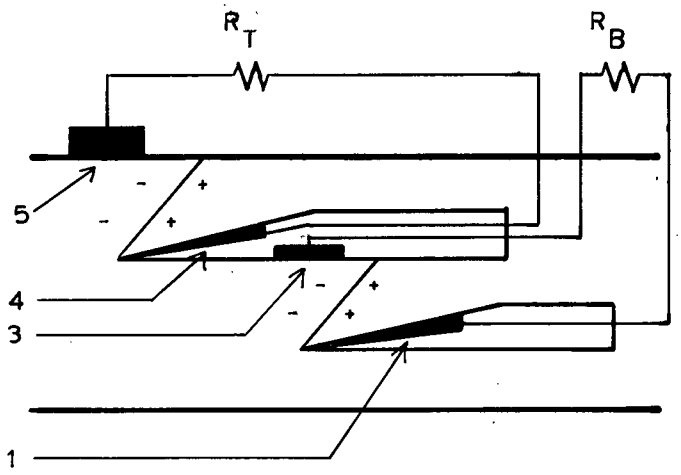

Figure 5.6 Configuration and electrode numbers for the two wedge bow shock generator experiments

signals from the top shock compared favourably with the previous measurements on a single shock. For the bottom shock however the signals were consistently of the reverse polarity, or very small during the time the framing camera pictures showed the bottom shock to be well established. Despite this unexpected result for the bottom wedge the V-I characteristic was measured for the top shock by varying the load resistor from shot to shot. The results, shown in Figure 5.4 and Figure 5.5 indicated an effective internal resistance of about 2.8±.5 Ohms. At low resistances it was also found that a small voltage of the expected polarity was generated by the bottom shock.

A number of attempts were made to improve the open circuit signal from the bottom wedge. Two of the

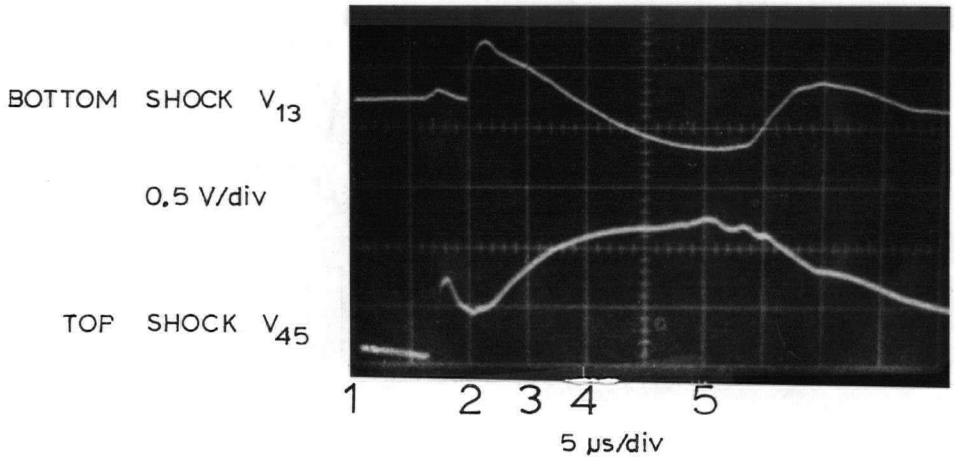

SHOCK VOLTAGES
(SEE FIG. 5.6 FOR ELECTRODE NO.)

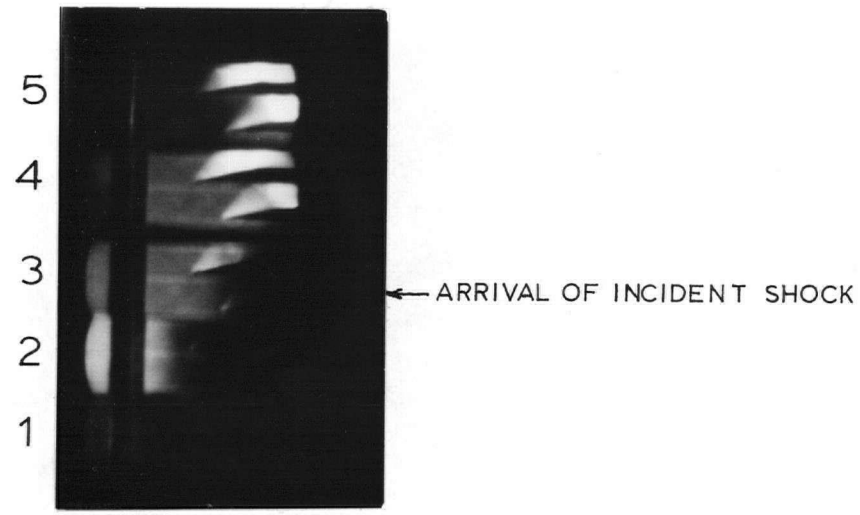

FRAMING CAMERA PHOTOGRAPH
(TIMING SHOWN ABOVE)

Figure 5.7 Two wedge open circuit voltage (across 100Ω) and framing camera pictures

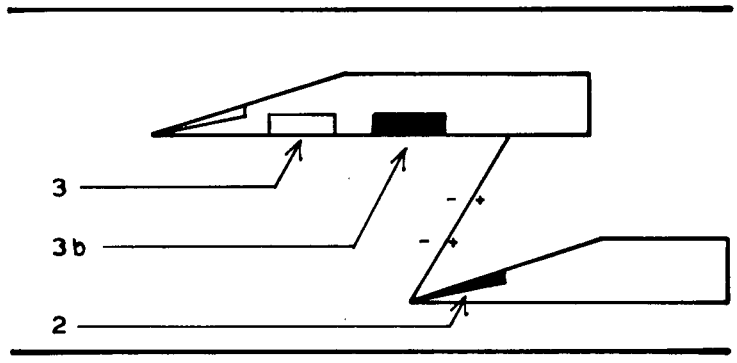

a) Top wedge moved forward one inch and a new electrode added

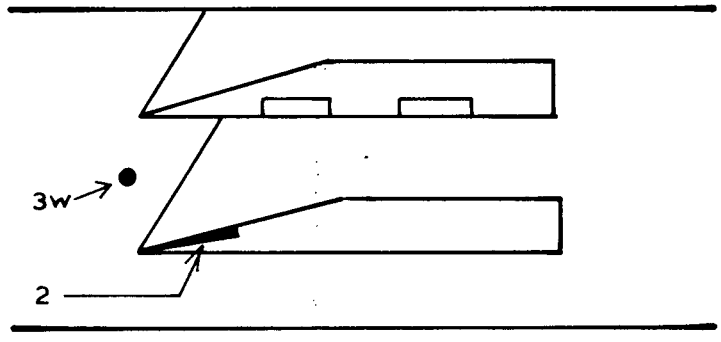

b) Voltage measured to a small electrode on the wall with the wedges lined up nose to nose

Figure 5.8 Two of the configurations that were tried while attempting to improve the bottom shock signal

configurations that were tried are shown in Figure 5.8. In the first one the top wedge was moved a distance of one inch upstream, and a new electrode added to the underside. In the second case the voltage was measured from the number 2 electrode to a small electrode mounted in the wall of the test section, ahead of the standing shock. Attempts were also made to improve the signal by tilting the nose of the upper wedge down a few degrees. None of these configurations was found to produce ,consistently, a voltage of the expected polarity

during the time the standing shock was well established.

5.2 SERIES CONNECTED SHOCK GENERATORS

To see if the voltage from a system of bow shock generators could be increased the two generators were connected in series by externally shorting the negative lead of one generator to the positive lead of the other and measuring the voltage across the pair. A schematic representation of this experiment is shown in Figure 5.9 part B. For the first experiments with the two generators connected in series the output was measured open circuit (across large load resistances). In these experiments the voltage measured across the pair of shocks was never greater than that across the top shock alone.

Another set of series connection experiments was carried out with a much larger load (smaller resistance) on the generators. Since a better voltage had been measured across the bottom shock alone when it was loaded with 2.8 Ohms, it was hoped that this change would increase the contribution of the bottom shock to the total signal. A smaller load resistance should also tend to reduce the effect of parasitic leakage currents through the plasma between electrodes 3 and 5.

Typical results for these experiments are shown in Figure 5.9. The voltage across each shock was first measured separately as shown in part A. A load resistor roughly

The scale on all three oscillograms is 0.5 V/div. and 5 μs/div. Arrows on the oscillograms indicate the time during which both standing shocks are well established.

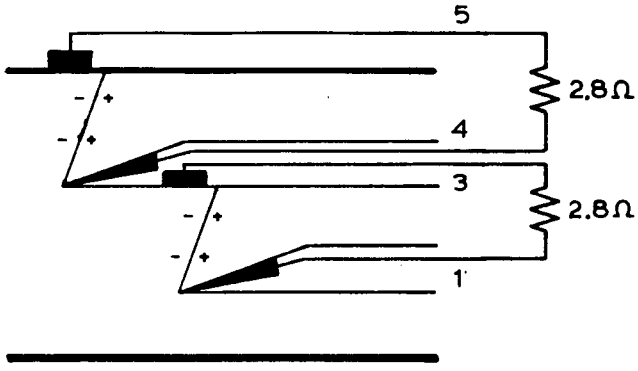

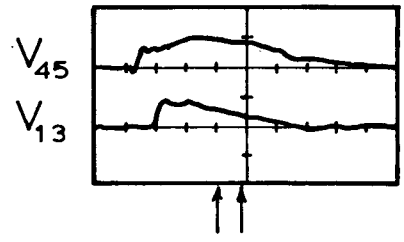

a) Voltage across each shock separately

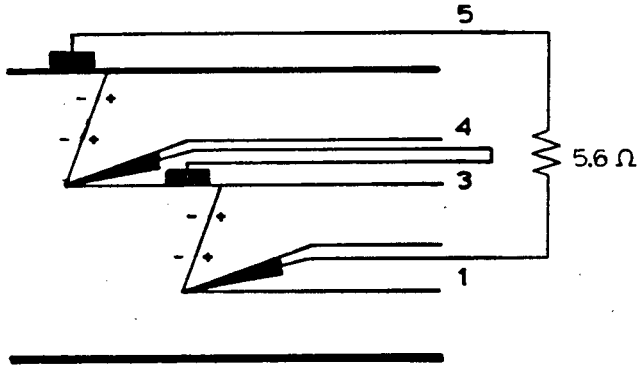

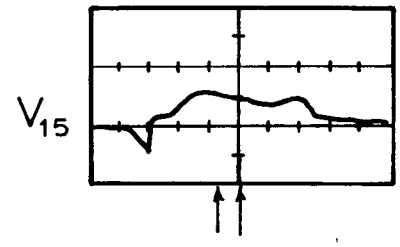

b) Voltage across both shocks in series

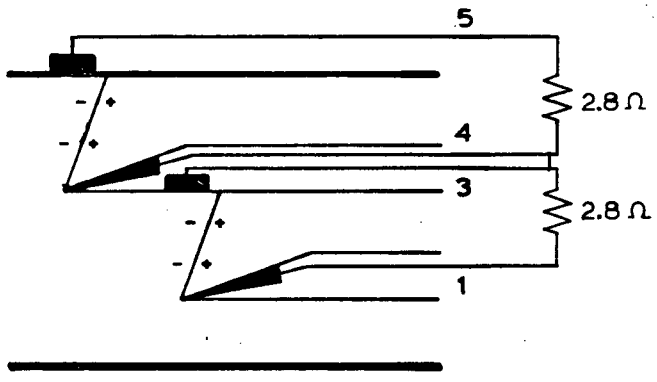

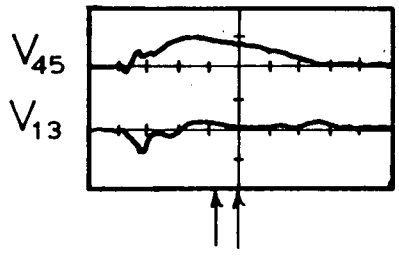

c) Effect of series connection on the voltage of each shock

Figure 5.9 The series connection experiments

matched to the internal impedance of the generator was used for maximum power transfer into the load. The two generators were then connected in series, keeping the load matched as shown in Figure 5.9 part B. Once again the voltage measured across the pair of shocks in series was not found to be significantly greater than the voltage across the top shock alone.

To observe the effect of the series connection on the output of each shock, the generators were connected as shown in Figure 5.9 part C. The results show that the signal from the top shock is changed little by the connection but that the shape of the bottom signal is quite different. The oscillogram also shows that the voltage between electrodes 1 and 3 is much reduced during the time the standing shocks are well established.

5.3 PARALLEL CONNECTED SHOCK GENERATOR

If several bow shock generators are connected in parallel it may be possible to increase the current delivered to a load over that supplied by a single generator. In order to test this concept an experiment was designed where the two generators could be connected in parallel. Since the voltage from the bottom shock was always much smaller than that from the top, a simple parallel connection of both generators into a single matched load would not work. In that case a fraction of the power from the top generator would be dissipated in the

plasma of the bottom generator instead of being delivered to the load. To demonstrate increased current in a load, a voltage divider load connected as shown in Figure 5.10 was

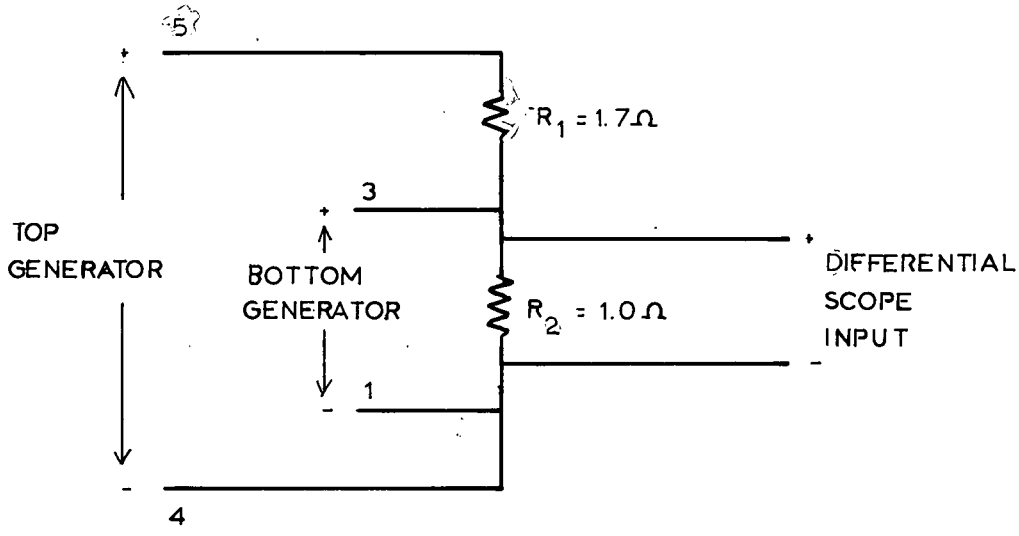

Figure 5.10 Loading of the generators used for the parallel connection experiments

used. The output from the top generator was applied across both resistors, which were chosen to match the internal resistance of the top generator. The voltage divider ratio was chosen so that when the bottom generator was connected to the small resistor, the power transfer to the load was a maximum. By measuring the voltage across the 1 Ohm resistor the current delivered to this part of the load could be determined. Figure 5.11 shows a comparison of the voltage across R when only the top generator was connected and then when both generators were connected in parallel. While the

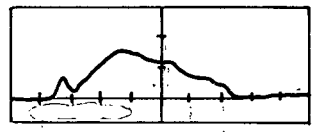

0.1 V/div
5 μs/div

VOLTAGE ACROSS R_2
TOP GENERATOR ONLY

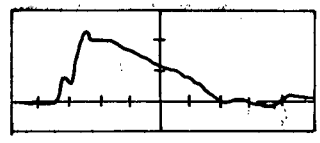

0.1 V/div
5 μs/div

VOLTAGE ACROSS R_2
BOTH GENERATORS IN PARALLEL

Figure 5.11 Output of single generator compared to output of parallel connection of both generators

generator load is not set up to extract maximum total power this experiment demonstrates that power output is increased when bow shock generators are connected in parallel.

5.4 REFLECTED OBLIQUE SHOCK GENERATOR

It may be possible to increase the voltage output of a system of generators and utilize the flow more efficiently by extracting power from the standing oblique shock and from successive reflections of this shock from the walls. The voltage could be increased by connecting the output from these shocks together on series. To test this possibility a system consisting of a single standing shock and its first reflection from the wall was investigated. In these experiments a symmetric wedge with one electrode on the leading edge was

used. Two electrodes were mounted on the wall one ahead of the first shock produced by the wedge and one in the region behind the reflected oblique shock as shown in Figure 5.12. The details of this generator system are described in Chapter 4.

Before the experiments on a series connection were done the first shock produced by the wedge was tested as an individual shock generator, without the reflected shock. The voltage was measured open circuit (across 100 Ohms) between electrodes 4 and 5 (see Figure 5.12) and was found to be $1.0V \pm 0.1V$. This is in good agreement with the previous results from single shock experiments.

To test the concept of connecting the first shock and its reflection from the wall together in series the voltage was measured from electrode 5 to electrode 2 (see Figure 5.12). Once again a 100 Ohm load was used. It was found that this voltage was less than 0.1V, much smaller than that across the first shock alone. Figure 5.12 shows a typical signal. While this result was somewhat unexpected it was similar to a result obtained much earlier during the experiments on single standing shocks.

Before it was recognized that it was important to mount the bottom wedge outside the boundary layer it had been mounted on the floor of the test section as shown in Figure 5.12. In this configuration the voltage across the shock was measured between an electrode on the front of the wedge and

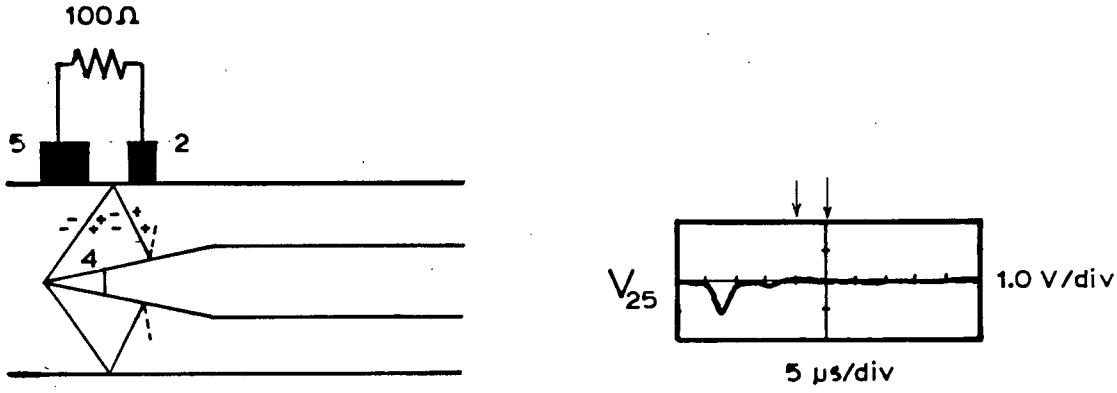

a) Series addition across a shock and its reflection. Arrows indicate the time during which the standing shocks were observed to be well established from framing camera photographs.

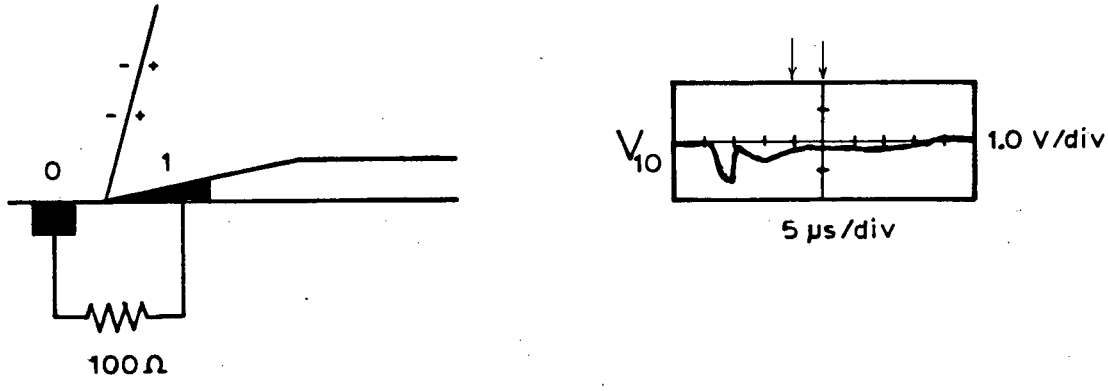

b) Early measurement of the voltage across a single standing shock

Figure 5.12 A comparison of the results of the reflected shock series addition signal and the early single shock experiments

one mounted on the wall well ahead of the shock. This voltage, as shown in Figure 5.12, was observed to be very small and of the opposite polarity to that expected from the other single standing shock experiments.

In both experiments the two electrodes were mounted one on each side of the shock front. However they were embedded in the same boundary layer and the voltages were found to be much smaller than those measured in other geometries. It therefore appears likely that the two electrodes are connected electrically through the boundary layer where the flow is subsonic.

In order to gain further insight into this particular configuration of shocks the voltage across the reflected shock alone was also measured. The open circuit (100 Ohms) voltage was obtained between electrode 4 and electrode 2 as shown in Figure 5.13. It was found to be 0.9V±0.1V and to have opposite polarity to that expected from the shock voltage across the reflected shock.

This unexpected signal is discussed along with the other results in the next chapter.

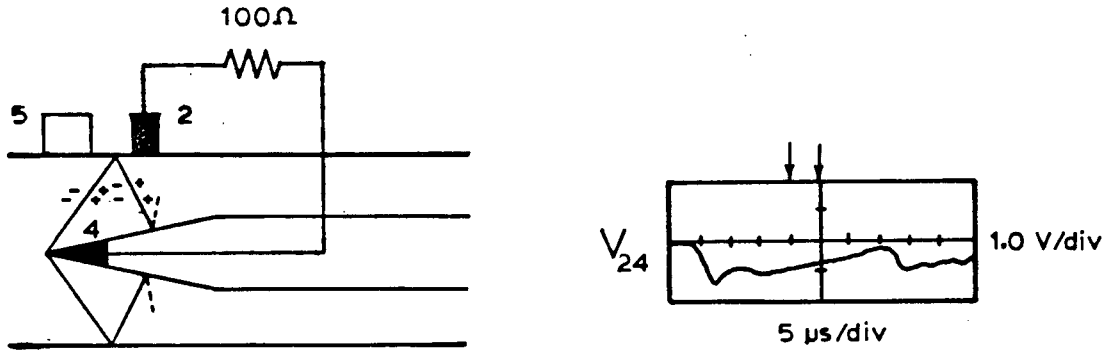

Figure 5.13 The reflected oblique shock voltage

CHAPTER 6. INTERPRETATION OF RESULTS

6.1 SUMMARY OF RESULTS

The results described in the previous chapter partly confirmed our understanding of bow shock generators and were partly unexpected. When trying to interpret the results, it is important to bear in mind that the experiments were carried out with one particular set of supersonic flow conditions, which may be summarized as follows:

$$T_1 = 10{,}300 \text{ K}$$

$$\rho_1 = 5.3 \times 10^{-5} \text{ gm/cm}^3$$

$$p_1 = 1.5 \times 10^{6} \text{ dynes/cm}^3$$

$$\alpha_1 = 2.7\%$$

$$n_{e1} = 2.1 \times 10^{6} \text{ cm}^{-3}$$

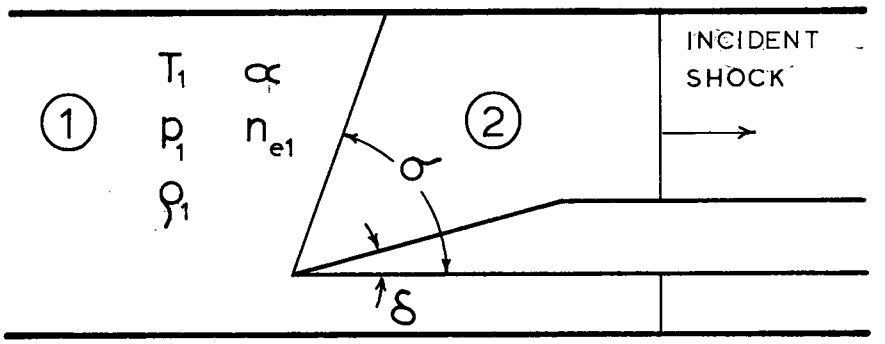

For wedges with an angle $\delta=12°$ as used in these experiments, the shock angle was measured to be $55°\pm2°$. The oblique shock in these experiments therefore had a Mach number of about 1.3.

In general there was a considerable shot to shot variation in the observed electrical signals, both in the magnitude and the shape of the signals.

The open circuit voltage across a single standing shock created by a wedge was usually $0.95V\pm0.1V$. For the bottom shock in the two wedge experiment however, a smaller less steady voltage,which sometimes even switched polarity, was

measured. When the load on a single shock generator was varied, the output voltage at maximum power transfer was found to depend on the electrode separation (d). When the electrodes were mounted at the largest practical separation (d=2 cm) the generator was found to have a maximum power output of 53 mW and an effective internal resistance of about 5.5±.5 Ohms. When the distance between the electrodes was reduced to d=1 cm the maximum power output increased to 90 mW and the generator was found to have an effective internal resistance of about 2.8±.5 Ohms.

A series connection of two shocks that were one above the other in the flow did not produce a larger voltage than that measured from one of the shocks alone. A parallel connection of the two shocks did however show a small increase in output current.

Measurements made on a shock and its reflection from the wall showed the voltage across the first shock to be in good agreement with other single shock measurements. The voltage across the shock reflected from the wall however was found to be opposite in polarity to that expected.

6.2 SHOCK ANGLE

The measured shock angle, σ, (see Figure 6.1) can be compared with the value predicted by oblique shock theory. In this calculation one assumes that the flow behind the shock is parallel to the wedge surface. The initial velocity of the

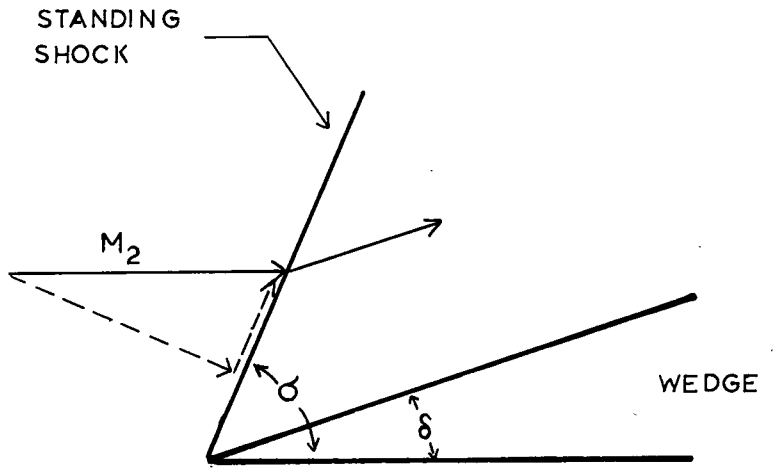

Figure 6.1 Oblique shock

supersonic gas is broken into two components. The velocity component parallel to the shock front is unchanged across the shock, while the velocity component perpendicular to the shock front undergoes a jump across the shock. The velocity jump for the perpendicular components is governed by the usual shock relations. In this way one can relate the shock angle, σ , to the incident Mach number (M_2) and the wedge angle δ. In the case of partially ionized flow, the normal shock relations are no longer applicable, as was mentioned in Chapter 2. A program has been written in the lab however, which by means of an iterative technique, calculates the flow parameters behind a normal shock wave in partially ionized argon (see appendix A). By applying these results to the perpendicular component of velocity across the oblique shock, the shock angle, σ , can be found as a function of M_2 and δ (see Table 1, in Section 6.3). An oblique shock program has also been written in this lab[18] which tabulates all the flow

parameters behind the oblique shock, and the shock angle for given initial conditions.

For the flow conditions in the shock tube, and a wedge angle of 12 degrees the oblique shock angle was calculated to be 46°. The measured value of the angle was 55°±2°. This may indicate that the flow behind the incident shock actually had a somewhat lower Mach number than that calculated from the speed of the incident shock. Alternatively, since the program does not take account of the finite relaxation rate for ionization in the gas behind the standing shock, this effect may produce a different shock angle than that predicted by the program.

6.3 OPEN CIRCUIT VOLTAGE

The open circuit voltage across the shock can be described with a fairly simple model, starting with the generalized Ohms law[19]. In one dimension with no magnetic fields present it may be stated as

$$-\frac{j}{e}\left\{n_i\varepsilon_{ie}(\varepsilon_{io}+\varepsilon_{eo})+n_o\varepsilon_{io}\varepsilon_{eo}\right\} \qquad (6.1)$$

$$= -(\varepsilon_{io}-\varepsilon_{eo})\,\text{grad}\,p_e - n_i(\varepsilon_{io}+\varepsilon_{eo})eE$$

where

j = current density

p_e = electron pressure

$\varepsilon_{kl} = \frac{4}{3}\sqrt{\left[\frac{8}{\pi}kT\left(\frac{M_kM_l}{M_k+M_l}\right)\right]}Q_{kl} \equiv$ friction coefficient

Q_{kl} = collision cross section

n_i, n_e, n_o = ion, electron, and neutral number densities

For the case of a standing shock there will be a large grad p_e term which will cause a charge separation between the

ions and the more mobile electrons. In the open circuit, steady state situation the current will be zero and the gradient term will be balanced by an E field caused by the charge separation. Since $\varepsilon_{io} >> \varepsilon_{eo}$ and $n_e = n_i$, the E field may be written as

$$E = -\frac{\text{grad } p_e}{en_e} = -\frac{1}{en_e}\frac{d}{dx}(n_e k T_e)$$

$$E = -\frac{k}{e}\left\{T_e \frac{d}{dx}(\ln n_e) + \frac{d}{dx} T_e\right\} \tag{6.2}$$

The potential across the shock may be found by integrating the E field from one side of the shock to the other.

$$\phi = \int_1^2 -E\,dx = \frac{k}{e}\int_1^2 T_e\, d(\ln n_e) + \frac{k}{e}\int_1^2 dT_e \tag{6.3}$$

For the integration the shock structure assumed by Jaffrin[2] was used. A schematic of the shock structure is shown in Figure 6.2. Since the charge separation between ions and electrons is small compared to the atom shock thickness, n_e

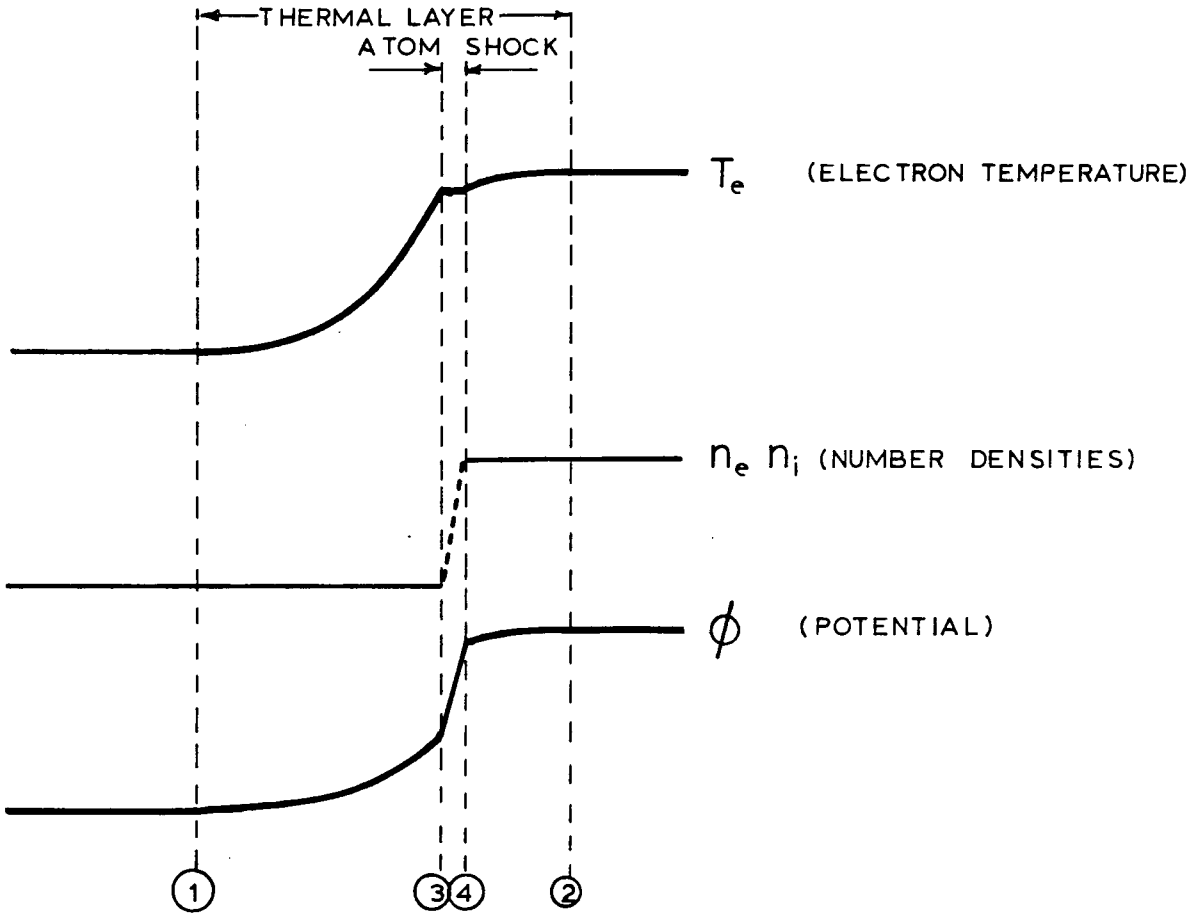

Figure 6.2 The model used for the shock structure

may be assumed to be constant everywhere except in the shock. The electron temperature begins to rise in the thermal layer ahead of the shock because of the high thermal conductivity of the electrons. Across the shock however, T_e is assumed to be constant. The integral may therefore be evaluated and the potential given as:

$$\phi = \frac{k}{e} T_{e4} \ln\left(\frac{n_{e4}}{n_{e3}}\right) + \frac{k}{e}(T_{e2}-T_{e1}) \tag{6.4}$$

Finally, Jaffrin's analysis shows that after the shock the electron temperature rises only a small amount so that T_{e4} may be approximated by the final electron temperature T_{e2}. Assuming that the flow is in equilibrium before and after the thermal layer, and that the ionization is frozen through the atom shock, the final result for the potential is

$$\phi \approx \frac{k}{e} T_2 \ln\left(\frac{\rho_2}{\rho_1}\right) + \frac{k}{e}(T_2-T_1) \tag{6.5}$$

with the temperature expressed in eV, the voltage across the shock can be written as

$$V \approx T_2(eV) \ln\left(\frac{\rho_2}{\rho_1}\right) + \Delta T_{21}(eV) \tag{6.6}$$

This voltage across a standing shock may be calculated from the flow state ahead of and behind the shock as tabulated by the oblique shock computer program (see Table I). For the case of the incident flow in these experiments the voltage predicted by this simple model is about 0.5V as compared to

Wedge angle δ°	Shock angle calculated σ°	Shock angle measured σ°	Shock voltage calculated	Shock voltage measured
8.9	43		0.36	
10.8	45		0.43	
12	46.4	55	0.49	0.95
14.1	49.0		0.58	
16.8	53		0.70	
20.6	61		0.90	

Table I Calculated and measured parameters for the shock generator

the measured value of 0.95V. The discrepancy may to a large extent be caused by the plasma sheaths at the electrodes. The behaviour of these sheaths for flat probes in supersonic flow is complicated and has not been well understood so no attempt was made to include them in this model.

6.4 INTERNAL RESISTANCE

As an estimate of the internal resistance of the generators the bulk resistance of the plasma between the electrodes was calculated. Using the generalized Ohms law (equation 6.1) with no magnetic fields or pressure gradients,

the bulk conductivity may be expressed as:

$$j = \frac{n_i \varepsilon_{ie} e^2 E}{n_i \varepsilon_{ie} \varepsilon_{io} + n_o \varepsilon_{io} \varepsilon_{eo}} = \sigma_{dc} E \tag{6.7}$$

where once again ε_{eo} has been neglected compared to ε_{io}. The conductivity may thus be expressed as:

$$\sigma_{dc} = \frac{e^2 n_i}{n_i \varepsilon_{ie} + n_o \varepsilon_{eo}} = \frac{3}{4} \frac{1}{\sqrt{\left(\frac{8}{\pi} kTM_e\right)}} \frac{e^2 n_i}{n_i Q_{ie} + n_o Q_{eo}} \tag{6.8}$$

The cross sections Q_{ie} and Q_{eo} were calculated from Arzimovich to be $Q_{ie} = 3.8 \times 10^{-13}$ cm^2, $Q_{eo} = 1.0 \times 10^{-16}$ cm^2. Using the temperature and number densities ahead of the shock where the conductivity is lowest, a value of $\sigma = 10.0$ mhos/cm was calculated. This was considered to be only an estimate, since the cross sections are only approximate, but it is in line with conductivities measured by Lin, Resler and Kantrowitz[21] under similar conditions of about 30 mho/cm.

The area of the electrodes in these experiments was about 2 cm^2 and for the top wedge generator the electrode spacing was about 1 cm. Using the above estimate for the conductivity, the bulk plasma resistance of the top generator would be no more than 0.1 Ohm. The measured value of the

effective internal resistance for this generator was about 2.8 Ohms, and the internal resistance increased by about a factor of two when the bulk plasma length was doubled. The discrepancy between measured and calculated resistamce may be due to the fact that ionization equilibrium had in fact not been reached during the test time. Lin, Resler and Kantrowitz, in their experiments, noted that in some cases the conductivity was still rising at the end of the test time, and therefore full equilibrium conductivity had not been reached. Their measured conductivities for these cases were as much as an order of magnitude below the theoretical values. It may therefore be, that in the bow shock generator measurements the conductivity has not reached its maximum equilibrium value, and thus the bulk resistance was still signficant. An alternative explanation is to assume that a significant contribution to the total resistancce comes from the thermal, electrical and flow boundary layers near the electrodes. It is difficult to assess their influence quantitatively however, as long as their exact extent and physical properties are not known.

From the variation of output voltage at maximum power, with distance, information could also be derived about the approximate field strength in the cold plasmas.

6.5 BOTTOM SHOCK

The bottom shock in the two wedge experiments was found to give a small unsteady open circuit signal(between electrodes 1 and 3 in Figure (5.6)), which sometimes even switched polarity. Since a good signal was obtained between the bottom wedge and an electrode in the top lid of the test section (electrodes 1 and 2 in Figure 5.6), the problem can be presumed to lie with the top wedge, or the electrode on the underside of this wedge (electrode 3). The boundary layer on the underside of this wedge will be different from that on the wall. Particularly late in the test time, the boundary layer on the wall will be thicker and more developed. This might affect the electrode or the plasma sheath in front of the electrode on the wall differently than the one on the wedge. Another possibility is that there was some spillage of hot plasma around the edge of the wedge, from the region behind the oblique shock of the top wedge. Since the tips of the wedges are always microscopically blunt, a small portion of the standing shock will be detached. This may allow some hot gas from the stagnation point to flow out under the top wedge. In some of the framing camera photographs, a faint glow was noticed along the bottom of the wedges. This was not consistently observed however, and it was difficult to tell whether or not the luminosity truly represented hot gas from the nose of the wedge. Finally, it might be possible that there existed a path between the two electrodes through the

boundary layers which line the vertical walls of the shock tube. If this were the case, moving the upper electrode from the top lid to the middle wedge would simply shorten the leakage path through the boundary layer.

6.6 SERIES CONNECTION

In experiments with the bow shock generators connected in series the output voltage measured across both shocks was never greater than that across the top shock alone. Once again to treat this problem properly the effects of the sheaths at the electrodes would have to be considered. A qualitative argument might be given as follows however.

Beginning at point 4 in Figure 6.3 the potential along the dotted line would drop through the first shock, then it might vary slightly from there to the next shock where it would rise again to roughly the same value. The resultant potential between electrodes 1 and 4 would be quite small. When electrode 3 is shorted to electrode 4 it may be that both electrodes assume the potential that electrode 4 had before the connection was made. The sheath in front of electrode 3 might then adjust itself, increasing the voltage drop across the sheath so that along a path from electrode 4 to electrode 1, passing through electrode 3 and the bottom shock, the net potential rise is small.

It should be pointed out that although the results from a series connection in the present experiments are discouraging,

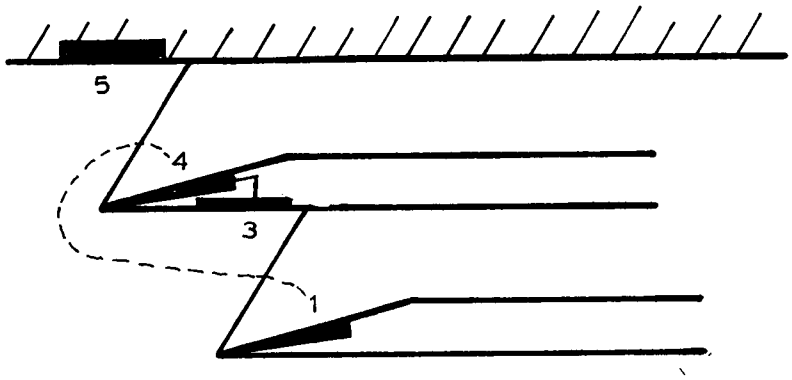

Figure 6.3 Series connected shocks

the poor signal from the bottom shock, and the variation in voltage signals from shot to shot, make it hard to draw a firm conclusion.

6.7 PARALLEL CONNECTION

In the case of a parallel connection of several generators it does appear that there may be some opportunity for an increase in current extraction. The difference in effective internal resistances between large and small standing shocks could make a number of small shock generators an attractive way to extract energy from a flow.

6.8 REFLECTED OBLIQUE SHOCK

In the experiments on the reflected shock, the attempts to add the voltages across an oblique shock and its reflection from the wall gave a very small signal. As was pointed out in Chapter 5 there was a similarity between this experiment and one in which a wedge and an electrode were mounted on the floor of the test section. The physical similarity of the flow in both situations is shown in Figure 6.4. In both cases the two electrodes are located close together in the boundary layer along the wall of the tube. If the temperature in the boundary layer is such that the gas has high conductivity then the two electrodes will be electrically shorted through the boundary layer and very little voltage will be measured between them.

In the case of the wedge mounted on the floor of the test section, the small voltage observed was actually of the opposite polarity to that expected from the voltage across the shock. It may be possible to explain this in terms of boundary layer separation since the shock may cause the boundary layer to separate from the wall upstream of the wedge[22]. If this were to happen, hot gas from behind the shock might be drawn forward under the boundary layer and brought to rest in a very hot stagnation state immediately above the electrode which is mounted in the floor. This electrode would then be hotter than the one on the wedge, and the polarity of the voltage observed between the two electrodes would be the

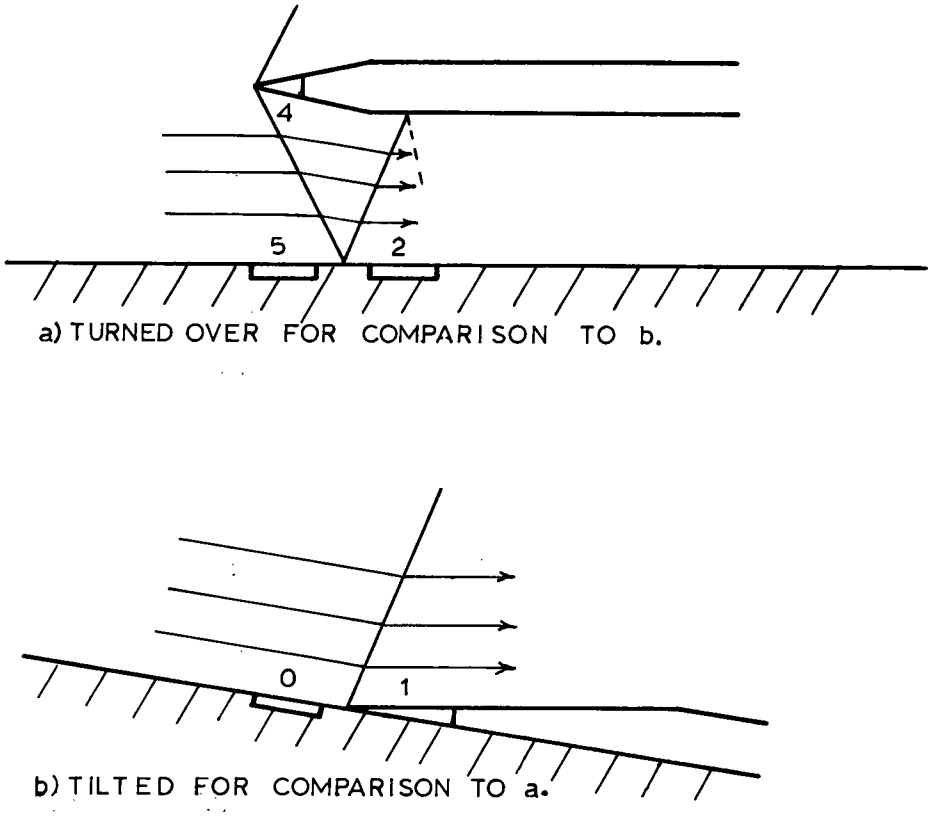

Figure 6.4 A comparison of the reflected shock experiment and the floor mounted wedge experiment

reverse of that expected from the shock voltage.

An interpretation of the measured voltage across the reflected shock alone can also be given in terms of the short circuiting effect of the boundary layer. Since the two electrodes on the wall are shorted together by the boundary layer the voltage between the electrode behind the shock and the nose of the wedge (V_{24}) will be the same as the voltage between the electrode ahead of the shock and the nose of the wedge (V_{54}).

A path from electrode 2 to electrode 5 and then through the shock to electrode 4 would give a signal opposite in

polarity to that expected across the reflected shock itself. The fact that the voltage (V_{24}) measured in this experiment was about the same magnitude as that measured across the first shock (V_{45}) indicates that in measuring V_{24} one most likely simply measures the voltage across the first shock.

Because of the electrical connection between the electrodes through the boundary layer in these experiments no firm conclusions can be drawn about the feasibility of series addition of successive shocks. If a longer test time were available it might be feasible to space two shocks farther apart along the tube so that the electrodes were not shorted through the boundary layer.

CHAPTER 7. EFFECTIVENESS AND SYSTEM ANALYSIS

One application for bow shock generators would be as a topping system ahead of a conventional turbine generation system. A conventional turbine is limited by thermo-mechanical effects to operate with gas flows at temperatures of about 1000K or cooler[23]. If one has a flow of gas with a high stagnation temperature, the temperature must be reduced before the flow can be used in a turbine. A series of bow shock generators provides a way of reducing the stagnation temperature by extracting energy from the flow. A bow shock generator can operate at these high temperatures because it has no moving parts and can therefore be run at temperatures given by metallurgical limits rather than thermal stress considerations. Furthermore it should be relatively easy to water cool the wedges so that very hot gas flows may be utilized.

A series of bow shock generators acting ahead of the conventional turbine would act as a topping system, not unlike that proposed for M.D.H. generators. In this way it may be possible to extract some energy from the flow at high temperature and thus increase the overall efficiency of the system. A schematic diagram for such a system is shown in Figure 7.1. It is assumed that the gas available to the system is at a very high stagnation temperature and that the

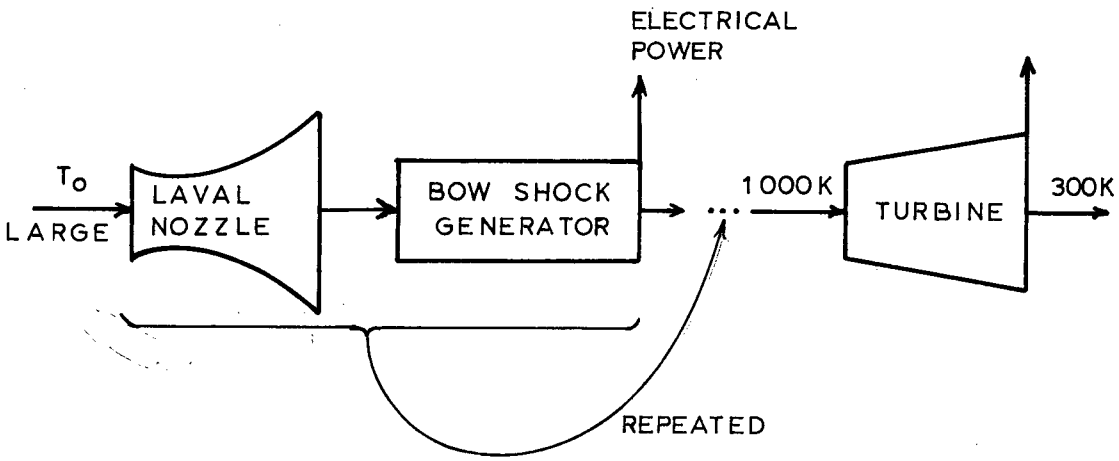

Figure 7.1 An example of a combined bow shock and conventional turbine generation system

coldest reservoir to which heat may ultimately be rejected is at a temperature of 300K.

Using this system as an example, a figure of merit can be calculated for the bow shock generator. To do this the concept of available energy is used. In any flow process the change in specific available energy of the flow can be defined as[24]

$$\Delta A = \Delta h + \Delta(\tfrac{1}{2}u^2) - T_c \Delta s = \Delta h_o - T_c \Delta s \qquad (7.1)$$

where

$\Delta h_o \equiv$ specific stagnation enthalpy change

u = flow velocity

Δs = specific entropy change in the process

T_c = temperature of the coldest reservoir available

If it is assumed that the bow shock generator runs adiabatically, then the change in stagnation enthalpy, Δh_o, is equal to the electrical energy extracted by the generator. The flow through the standing shock is however irreversible ($\Delta s \neq 0$). Whenever an irreversible process takes place the effect is to convert a certain amount of energy from a form in which it is completely available to a form in which it is completely unavailable and can no longer be extracted as work[24]. The amount of energy made unavailable depends on the entropy change in the process and on the temperature of the coldest reservoir at hand (T_c) to which heat may be rejected to do work. For an irreversible process the loss in available energy is given by $T_c \Delta S$, as indicated by the presence of this term in equation 7.1. In the system used as an example, T_c would be 300K. To calculate ΔS it is assumed that for the generator the shock is the major source of entropy change in the flow and so ΔS can be calculated from shock theory (see Appendix B for details).

As the flow passes through the generator energy is extracted but the flow suffers a loss in available energy. One figure of merit for the generator is called the effectiveness and is defined as the ratio of the energy

extracted from the flow to the loss in available energy of the flow.

$$\varepsilon = \frac{|\Delta W|}{|\Delta A|} \qquad (7.2)$$

where ΔW = specific energy extracted from the flow

The effectiveness compares the energy extracted by the device to the energy extracted by a reversible device operating between the same end conditions.

The effectiveness was calculated and used as one figure of merit for the operation of the experimental bow shock generators. Once again T_c was assumed to be 300K and the entropy change across the shock was calculated based on the strength of the oblique shock. For the highest measured power output from the generator (90mW) the effectiveness was calculated to be approximately 0.2 per cent.

While this figure may seem low it must be remembered that no other machines , except MHD generators (which have yet to overcome a number of scientific problems) are capable of operating in this high temperature region at all. The object of using bow shock generators ahead of conventional turbines is to reduce the stagnation temperature of the flow. Other means of lowering the stagnation temperature must also involve

a loss of available energy and do not have the compensating benefit of energy extraction.

To evaluate the bow shock generator a comparison was made between the loss of available energy caused by cooling a hot gas with a bow shock generator and the loss in available energy caused by cooling the gas by the addition of cold gas. In each case, one starts with the hot gas in its stagnation state (stationary). The gas may either be accelerated from the stagnation state to supersonic velocities in a Laval nozzle and then cooled with a bow shock generator, or a mass of cold gas may be added to the hot gas in the stagnation state, and the hot gas cooled by thermal conduction. In each case the gas was cooled to the same end stagnation temperature.

The losses in the bow shock generator depend on the Mach number at which it is operated. Since only one Mach number had been investigated experimentally a theoretical calculation was done to compare the losses from both methods of cooling as a function of Mach number. The Mach number used throughout these calculations is the Mach number of the standing shock (equal to the Mach number of the component of the flow perpendicular to the standing shock). The calculation was based on the flow conditions used in the experiments and the variation in Mach number would correspond to the use of generators with different wedge angles.

A model was assumed that allowed a prediction of the

output of the generator as a function of Mach number (see Appendix B for details of these calculations). At each Mach number the drop in stagnation temperature and the loss in available energy caused by the bow shock generator was computed. For comparison with mixing, an amount of cold (300K) gas sufficient to lower the stagnation temperature by the same amount was considered to be added to the flow in its stagnation state. The loss of available energy through irreversible heat flow from the hot gas to the cold gas was then computed for comparison (see Appendix B). The results are shown in Figure 7.2 as the available energy lost from one gram of hot gas which is put through either process. The loss in available energy for the bow shock generator is the change in available energy for the flow beyond the energy extracted. For reference, Figure 7.3 shows the energy extracted by the generator and its effectiveness as a function of Mach number. The available energy flow in such a system is illustrated schematically in Figure 7.4 assuming perfect ducting and perfect turbines. It can be seen from the energy balance that the two processes will just break even when the electrical energy extracted plus the energy extracted by the turbine in the bow shock system is equal to the energy extracted by the turbine in the mixing system ($A_{outbs}+A_{ex}=A_{outm}$), or alternatively, when the available energy loss in the bow shock system is equal to the available energy loss in the mixing system ($A_{lbs}=A_{lm}$). If the loss of available energy incurred

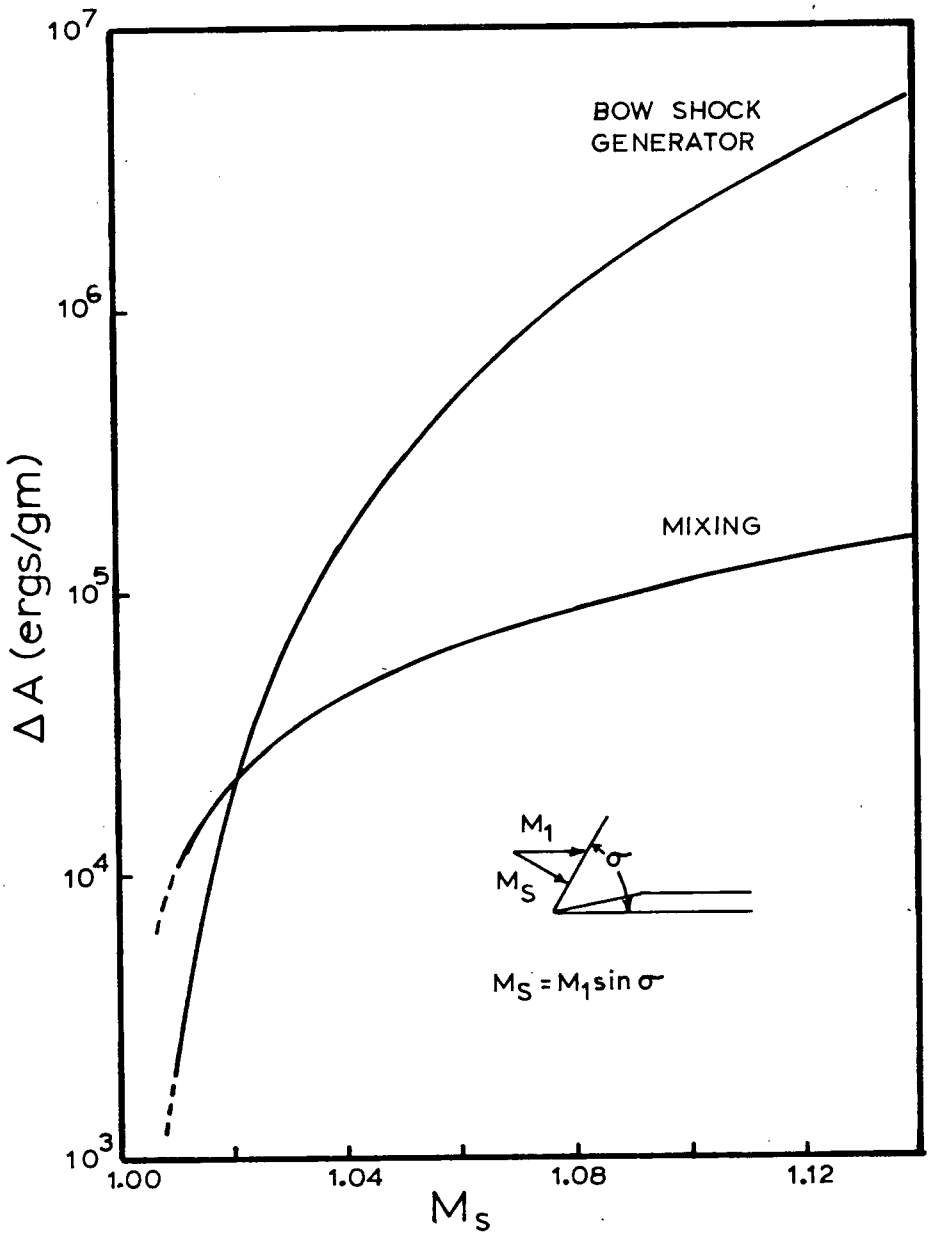

Figure 7.2 A comparison of the available energy lost from one gram of hot input gas (ΔA) in both the cooling processes (bow shock generator and mixing) as a function of the Mach number at which the generator is run

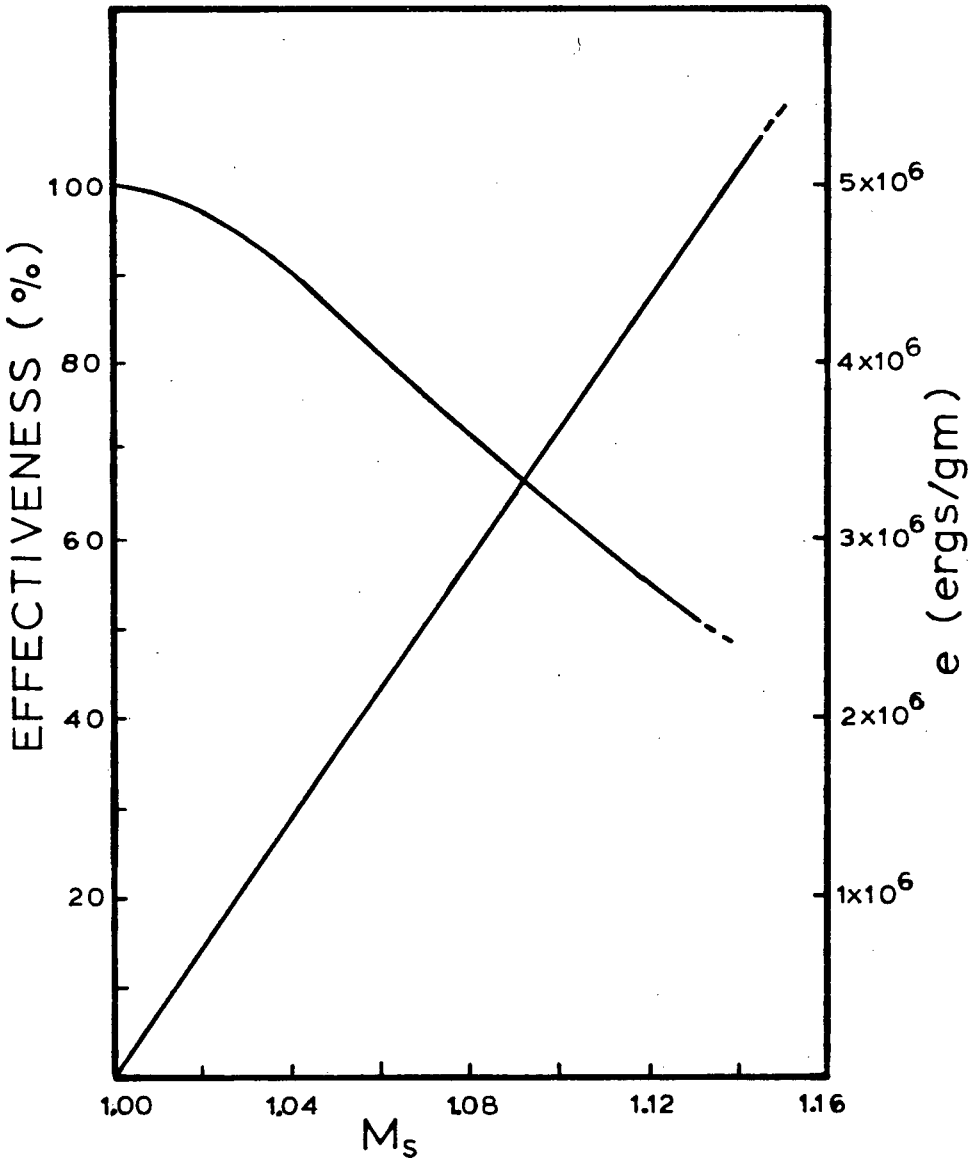

Figure 7.3 Energy extracted (e) and effectiveness of a bow shock generator as a function of Mach number (M_s)

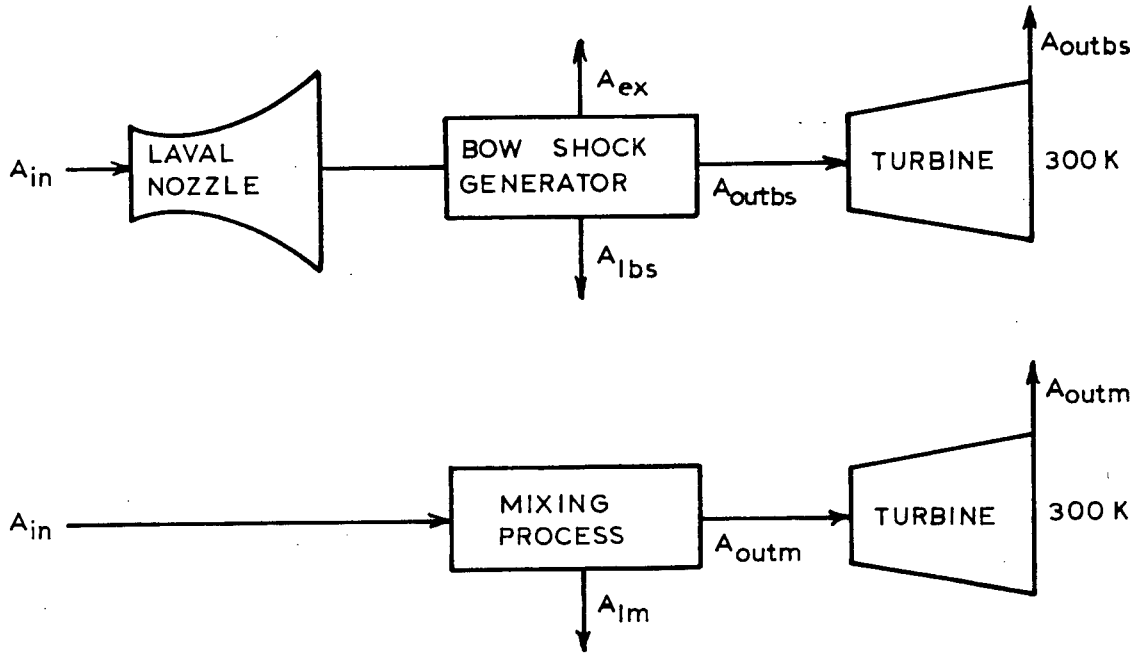

One gram of hot gas enters each process

A_{in} = available energy in one gram of hot inlet gas
A_{ex} = energy extracted in bow shock generator
A_{lbs} = available energy lost in bow shock generator
A_{outbs} = energy extracted by turbine in bow shock system
A_{lm} = available energy lost in mixing process
A_{outm} = energy extracted by turbine in mixing process

Figure 7.4 Available energy flow in the shock generator plus conventional generator system, compared to that in the mixing plus conventional generator system.

by the generator can be made less than that incurred by mixing the generator will be the more efficient means of cooling the flow. As can be seen from Figure 7.2 at low Mach numbers the bow shock generator appears more efficient.

This analysis has shown that if a bow shock generating

system were to be used as a topping system for a conventional generation plant, it would have to be run at very low Mach numbers. Mach numbers just greater than one are relatively easy to achieve. Unfortunately in this regime some of the assumptions in this model break down. It has been assumed that the shock accounts for all the losses in the bow shock system. At low Mach numbers however, heat loss to the walls, and friction in the ducting may be important as well. Another problem lies with the fact that the energy extracted from the flow in the experiments is less by a factor of 300 than that predicted by the model used in this analysis. A more thorough analysis, including these effects would have to be done before one could say that bow shock generators would be viable in this particular application.

CHAPTER 8. CONCLUSIONS AND SUGGESTIONS FOR FUTURE WORK

8.1 SUMMARY AND CONCLUSIONS

An overdriven detonation shock tube was built to produce a flow suitable for experiments on power extractions from standing shock waves. In most respects the shock tube met the requirements of these experiments. It produced a flow of gas in a well defined thermodynamic state that was supersonic and had a duration greater than 20 microseconds. Unfortunately the flow was not completely constant and uniform during all of this time. By inserting a suitable obstacle into the flow an oblique shock could be created across which the ionization in the flow was increased significantly. Most importantly the flow field was free of large electrical currents and voltages.

Using this shock tube, a number of preliminary experiments were carried out on single standing shocks. It was found that the open circuit voltage measured was higher by a factor of two than that calculated from theory using the model of Jaffrin. It is apparent that it is not sufficient to consider the potential across the shock as the only source of voltage between the two electrodes, and that the effects of plasma sheaths and flow boundary layers are important as well. The effective internal resistance of a shock generator was found to depend on the separation of the electrodes. The

values of resistance measured were considerably larger than values predicted from a calculation of the bulk conductivity of the plasma. Two possible explanations were advanced for this. It could be that the gas in the shock tube does not reach its full equilibrium conductivity during the test time. Alternatively this effect may be caused by resistances in the boundary layers, which vary with the positions of the electrodes in the tube.

The principle aim of these experiments was to investigate the possibility of increasing the output of bow shock generators by connecting together more than one generator. This possibility was tested in two different geometries.

In the first geometry two standing shocks, created by two wedges, stood physically in parallel across the flow. It was found that the output voltage of one of these shocks (the lower one) was consistently smaller than that of the other, and unless a large load (small resistance) was connected across this generator the voltage could even be of the opposite polarity. In the experiments which attempted to increase the output voltage by connecting these two shocks together in series, the total voltage across both shocks was never observed to be larger than that across one shock alone. When these two shock generators were connected in parallel it was shown that a small increase in output current could be obtained.

In the second geometry, a series connection between a

standing oblique shock, and its reflection from the wall of the shock tube was investigated. Attempts to add the voltages across the two shocks showed the total voltage to be very small. However it appears as if the electrodes on each side of the two shocks were shorted together through the boundary layer. This connection through the boundary layer also made it impossible to measure the voltage across the reflected shock alone, since the electrode on the wall behind the reflected shock was always shorted to the gas ahead of both shocks.

A study was also undertaken to define a figure of merit for bow shock generators, and the use of a figure called the effectiveness was proposed. Using the effectiveness, a preliminary analysis was made of a hybrid bow shock/conventional turbine generation system. It was shown that if bow shock generators are to be at all practical in this application they must be operated at very low Mach numbers to reduce the loss in available energy caused by irreversibilities in the shock. Unfortunately at low Mach numbers other losses which are not taken into account in this model may become important.

The experiments with multiple shocks were the first attempts to increase the power output from bow shock generators by connecting more than one generator together. The proposal of the effectiveness as a figure of merit, and the analysis of the performance of bow shock generators as a

topping system for a conventional generating plant were also original contributions.

8.2 SUGGESTIONS FOR FUTURE WORK

There are obviously some features of these experiments which are not completely understood, and would merit further investigation. The magnitudes and even the polarity of some of the voltages measures across shocks in this work cannot be understood in terms of the shock voltage alone. No attempt has been made here to try to include the effects of the plasma sheaths at each electrode, or the effects of the flow boundary layer. If the bow shock generator is to be more fully understood however, the relative importance of these effects must be determined, and some account of them included in the model. Further experiments might also attempt to determine more precisely the source of the high internal resistance, since this will be important in any attempt to increase the power output of bow shock generators.

To study possible applications of bow shock generators it would be useful to have a better model of the extraction of electrical power in a shock generator. With such a model a more detailed analysis of the hybrid generation system could be undertaken. At low Mach numbers, where this work indicates they should be run, the assumption that the shock wave accounts for most of the losses in the flow is no longer valid, and other losses must be taken into account.

Tests on bow shock generators should also be conducted in a continuous flow apparatus. This would remove some of the problems encountered with unsteady flow in these experiments, as well as allowing measurements in flows with a wider range of Mach numbers than those available in a shock tube. In a continuous flow machine the shock generators could also be moved physically farther apart so that they would not be electrically connected with short paths in the boundary layers along the walls. Alternatively one could try to use one of a number of methods developed for boundary layer control to interrupt the boundary layer between the electrodes.

BIBLIOGRAPHY

1. Petscheck, H. and Byron, S., Annals of Physics 1, 270-315 (1959).
2. Jaffrin, M.V., The Physics of Fluids 8, 606-625, (1965).
3. Tidman, D.A. and Burton, L.L., Physics Review Letters 37, 1397, (1968).
4. Ahlborn, B., Kwan, J. and Pearson, J., Proceedings of the Twelfth Annual Symposium on Shock Tubes and Waves, Jerusalem, (1979).
5. Ahlborn, B. and Kwan, J., U.S. Patent #877494, Applied February 13, 1978.
6. Kwan, J., Proceedings I.E.E.E. Conference, Monteray, May 1978.
7. Becker, E., Gas Dynamics, Academic Press, New York, (1968).
8. Ahlborn, B., Lecture notes Physics 507, University of British Columbia, (1974).
9. Ahlborn, B., Canadian Journal of Physics 53, 976-979, (1975).
10. Resler, E.L., Lin, S. and Kantrowitz, A., Journal of Applied Physics 23, 1390-1399, (1950).
11. Gaydon, A.G. and Hurle, I.R., The Shock Tube in High Temperature Chemical Physics, Chapman and Hall Ltd., London, (1963).
12. Muntenbruch, H., Physics of Fluids Supplement I 12, 1-11, (1969).
13. Redfern, P. and Ahlborn, B., Canadian Journal of Physics 50, 1771-1776, (1972).
14. Courant, R. and Friedrichs, K.O., Supersonic Flow and Shock Waves, Interscience Publishers, New York, (1948).
15. Ahlborn, B. and Huni, J.P., Journal of Applied Physics 40, 3402-3404, (1969).
16. Huni, J.P., Ph.D. Thesis, University of British Columbia, (1970).
17. Redfern, P., M.Sc. Thesis, University of British Columbia, (1971).
18. Kwan, J., Ph.D. Thesis, University of British Columbia, (to be published).
19. Wienecke, R., Zeitsch Naturforschung 18a, 1151, (1963).
20. Arzimovich, L.A., Elementary Plasma Physics, Blaisdell Publishing Co., Waltham Mass. (1965).
21. Lin, S.C., Resler, E.L. and Kantrowitz, A., Journal of Applied Physics 26, 95-109, (1955).

22. Chapman, A.J. and Walker, W.F., Introductory Gas Dynamics, Holt Rinehart and Winston Inc., (1971).

23. Lee, J.F. and Sears, F.W., Thermodynamics, Addison Wesley Publishing Co., Reading Mass., (1963).

24. Drellishak, K.S., Knopp, C.F. and Cambel, A.B., Physics of Fluids 6, 1280-1288, (1963).

25. Bosnjakovic, F., Springe, W. and Knoche, K.F., Zeitsch Flugwiss 10, 413-424, (1962).

APPENDIX A CALCULATION OF THE THERMODYNAMIC STATE BEHIND AN IONIZING SHOCK

When a gas becomes partially ionized the simple equation of state for a calorically ideal gas is no longer applicable. Instead the enthalpy coefficient, g, is defined[9], where g(h,p) is a function of the thermodynamic state of the gas.

Using this equation of state and the conservation equations across a shock front the thermodynamic variables behind the shock may be found from the initial conditions ahead of the shock and the shock Mach number. However, this calculation assumes a knowledge of the enthalpy coefficient behind the shock, g_2, which is initially unknown. For an equilibrium final state, however, $g_2(h_2,p_2)$ is a well defined function of h_2 and p_2, so that an iterative technique may be used to find the final state[9]. This method operated by guessing a value of g_2 and then using it to calculate the final state from the shock relations and the equation of state. From the calculated final state a new value of g_2 is chosen and the process repeats itself until the iteration converges. Data for g(h,p) may be obtained from thermodynamic calculations using partition functions for the gas in question and the Saha equation[25].

To do this iterative calculation a computer program has been written in this lab by Joe Kwan[18]. The program tabulates a variety of thermodynamic variables behind shock waves in argon for given initial conditions and Mach numbers as high as

13. These values were used in a number of places throughout this work.

APPENDIX B. AVAILABLE ENERGY LOSS IN BOW SHOCK GENERATORS AND MIXING

B.1 INCIDENT FLOW PARAMETERS

The calculations in this section were based on the flow in the shock tube as it was used in the experiments. The parameters were calculated from shock theory applied to partially ionized argon and based on the observed Mach number (see Appendix A). For the flow state in the shock tube the conditions are:

$$p = 1.15 \times 10^{6} \text{ dynes/cm}^2$$

$$\rho = 5.3 \times 10^{-5} \text{ gm/cm}^3$$

$$T = 10{,}300 \text{ K}$$

$$u = 2.88 \times 10^{5} \text{ cm/sec}$$

$$M_2 = 1.58$$

$$h = 6.47 \times 10^{10} \text{ ergs/gm}$$

$$g = \gamma = 1.51$$

$$\dot{m} = \rho u = 15 \text{ gm/sec}$$

The corresponding stagnation state can be obtained from a Mollier diagram[26].

$$h_o = 1.06 \times 10^{11} \text{ ergs/gm}$$

$$T_o = 13{,}000 \text{ K}$$

$$p_o = 5.4 \times 10^{6} \text{ dynes/cm}^2 \simeq 5 \text{ atm}$$

B.2 STANDING SHOCK JUMP

The standing shocks investigated were assumed to be weak enough so that γ could be assumed to be constant across the shock. However since the flow was partially ionized the value of γ in the incident flow (γ=1.51) was used in place of the low temperature value. The temperature, pressure, and density behind the standing shock were then calculated as a function of Mach number from ideal shock theory with γ=1.51.

B.3 ENERGY EXTRACTED BY THE GENERATOR

It was assumed that the V-I characteristic of the generator was linear so that the maximum power output could be approximated by

$$p = \frac{V_{oc} I_{sc}}{4} \qquad (B.1)$$

where V_{oc} = open circuit voltage of the generator

I_{sc} = short circuit current of the generator

The open circuit voltage was predicted by the model expressed in Chapter six

$$V_{oc} = T_3 \ln\left(\frac{\rho_3}{\rho_2}\right) + \Delta T_{32}$$

where regions 2 and 3 are as shown in Figure B.1 and the

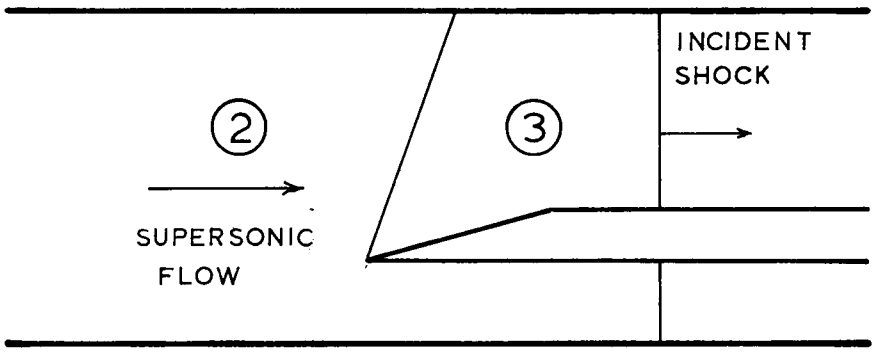

Figure B.1 Bow shock generator regions

temperatures and density ratio have been calculated as shown in the above section.

A prediction has been made of the short circuit electron current that would flow across the shock if it were diffusion limited . The result can be expressed in the form[4]

$$j = \frac{3.15\times10^{-12}\ \Delta(n_e T_{eV})}{\sqrt{(T_{eVavg})}} \quad \text{Amps/cm}^2$$

where
- j = short circuit density current
- $\Delta(n_e T_{eV})$ = the change in electron number density x the temperature product between regions 3 and 2
- T_{eVavg} = some intermediate temperature in the shock

The current predicted from the diffusion limit can be shown to be larger than the flux of incoming electrons in the flow for Mach numbers 1.01 or greater. Thus for all but the very weakest shocks the short circuit current is not diffusion limited. For the operating conditions of the shock tube the incident flux of electrons corresponded to a current density of 100 Amps/cm^2.

As an estimate of the short circuit current it was assumed that an electron gradient could be maintained in the shock and a diffusion driven current supported if only 10 per cent of the incoming electrons contributed to the short circuit current. The short circuit current was therefore assumed to be 100 Amps over the range of Mach numbers investigated. This was in fact higher by a factor of 300 than the short circuit current measured in the experiments.

The specific energy extracted from the flow at any Mach

number is simply the power predicted by equation (B.1) divided by the mass flux.

$$e = \frac{P}{\dot{m}}$$

$\dot{m}$ = 15 gm/sec in this case

Since the flow is assumed to be adiabatic the reduction in stagnation enthalpy is equal to the energy extracted.

$$\Delta h_o = -e$$

B.4 AVAILABLE ENERGY LOSS IN GENERATOR

The change in available energy across the shock is given by (see Chapter 7)

$$\Delta A = \Delta h_o - T_c \Delta s$$

where T_c = temperature of the coldest reservoir available

where Δh_o represents available energy extracted in the form of electrical power and $T_c \Delta s$ represents the loss in available energy incurred through the irreversible nature of the shock.

(B.2)

$T_c \Delta s$ = loss of available energy

The entropy jump in the shock may be calculated from the

general entropy change in any process proceeding from state (T_2,P_2) to state (T_3,P_3)[23].

$$\Delta s = c_p \ln \frac{T_3}{T_2} - R \ln \frac{P_3}{P_2}$$

Since the standing shock was assumed to be weak c_p and R were taken as constant across the shock although the values used were those at the elevated temperature of the incident flow.

The temperature and pressure ratios used were those previously calculated for the standing shock jump as a function of Mach number.

Having calculated the entropy increase as a function of Mach number, the loss in available energy for one gram of hot gas may be calculated from equation (B.2). This figure may then be compared to the available energy lost when one gram of hot gas is mixed with cold gas to cool it the same amount.

B.5 AVAILABLE ENERGY LOSS IN MIXING

For comparison the available energy loss was calculated if the flow was cooled from the stagnation state through the addition of cold gas. This means that the cold gas must absorb as much energy from the flow in the form of heat as the bow shock generator extracted as electrical energy. Instead of being accelerated to supersonic velocity in a Laval nozzle, the flow is isentropically brought to rest so that it is in

the stagnation state, and a mass of cold gas, sufficient to achieve the required cooling is added. The available energy lost from one gram of initially hot gas can then be calculated from the irreversible heat conduction.

An amount of cold gas is assumed to be mixed into one gram of hot gas at stagnation conditions in a process illustrated schematically in Figure B.2.

Before the cold gas can be mixed it must be compressed to the stagnation pressure. If the compressor is assumed to be isentropic the work done by the compressor is

$$W = m_c(h'_c - h_c)$$

The total change in available energy for the system (hot gas plus cold gas) from state 1 to state 3 is given by

$$\begin{aligned} \Delta A_{system} &= \Delta H - T_c \Delta S \\ &= h_o + H' - h_o - H - T_c \Delta S \\ &= W - T_c \Delta S \end{aligned}$$

where the variables are those defined in Figure B.2.

If the compressor is isentropic the work done on the fluid appears totally as available energy in the gas and the net result of the process is the loss of available energy through heat conduction ($T_c \Delta S$). Therefore the net change in available energy for one gram of hot input gas is given by the

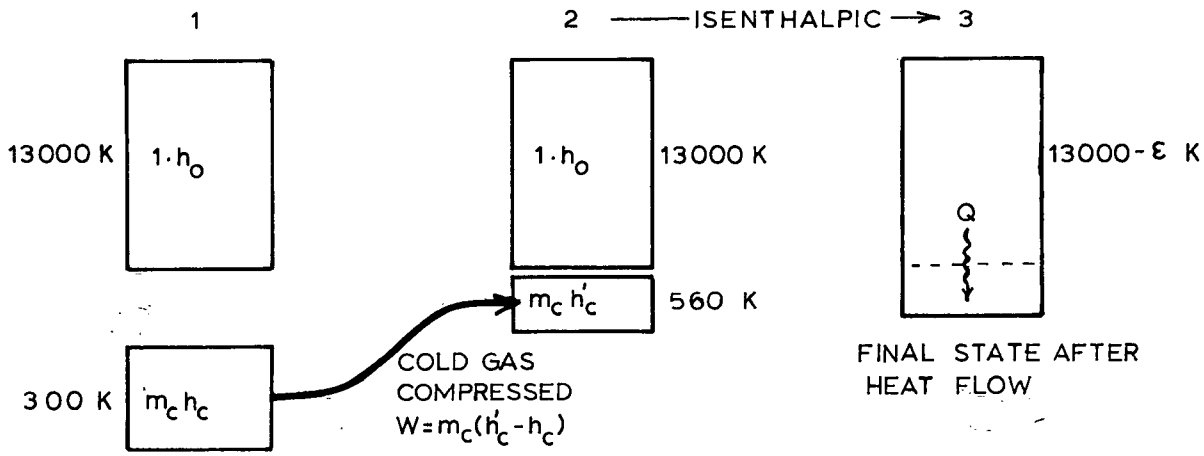

where ΔS = entropy change of the system

ΔH = enthalpy change of the system

h_c = specific enthalpy of cold gas before compression

h_c' = specific enthalpy of cold gas after compression

h_o = specific enthalpy of the hot gas

m_c = mass of cold gas added

W = work done by the compressor

ε = very small

Figure B.2 The mixing process

loss in available energy.

$$\Delta A = T_c \Delta S = \text{net loss in specific available energy due to mixing} \quad (B.3)$$

For the stagnation state outlined at the beginning of

this appendix the cold gas to be added must be isentropically compressed to 5 atmospheres which raises its temperature from 300K to 560K. The mass of compressed gas which must be added to one gram of hot gas is determined by the amount of heat that must be extracted from the hot gas:

$$Q = e = m_c \int_{560}^{(13,000-\varepsilon)\approx 13,000} c_p(T,5\ \text{atm})\,dT \qquad (B.4)$$

m_c = mass of cold gas

The integral was approximated numerically from the data for c_p[25]. The upper limit may be approximated as the stagnation temperature since in all cases here the amount of cooling is small.

The entropy change for the system due to this heat flow is given by

$$\Delta S = \frac{-Q}{13,000} + \int_{560}^{\approx 13,000} \frac{m_c c_p(T,5\ \text{atm})}{T}\,dT \qquad (B.5)$$

Once again the integral was approximated from data for c_p. The loss in specific available energy may then be calculated from equation B.3.

At each operating Mach number for the bow shock generator the energy extracted from one gram of flow has been computed. If this same amount of energy flows into the cold gas as heat, the available energy lost from one gram of hot gas in the

mixing process may be calculated from equations (B.4), (B.5), and (B.3). This may then be compared to the available energy loss for the bow shock generator.